Free Methionine Sulfoxide Reductase and its Contributions to Environmental Stress Response in *Komagataeibacter hansenii*

by

Rhys Bartlett

A thesis submitted to the
School of Graduate and Postdoctoral Studies in partial
fulfillment of the requirements for the degree of

Master of Science in Applied Bioscience

Faculty of Science

University of Ontario Institute of Technology (Ontario Tech University)

Oshawa, Ontario, Canada

December 2023

THESIS EXAMINATION INFORMATION

Submitted by: **Rhys Bartlett**

Master of Science in **Applied Bioscience**

Thesis title: Free Methionine Sulfoxide Reductase and its Contributions to Environmental Stress Response in *Komagataeibacter hansenii*

An oral defense of this thesis took place on December 7, 2023 in front of the following examining committee:

Examining Committee:

Chair of Examining Committee	Dr. Denina Simmons
Research Supervisor	Dr. Janice Strap
Examining Committee Member	Dr. Dario Bonetta
Thesis Examiner	Dr. Syed Qadri

The above committee determined that the thesis is acceptable in form and content and that a satisfactory knowledge of the field covered by the thesis was demonstrated by the candidate during an oral examination. A signed copy of the Certificate of Approval is available from the School of Graduate and Postdoctoral Studies.

ABSTRACT

Komagataeibacter hansenii (ATCC 23769) is a non-virulent acetic acid bacterium that forms cellulosic biofilms at the air-liquid interface of liquid media, serving as a model for biofilm forming pathogenic bacteria. In this thesis, the role of free methionine-R-sulfoxide reductase (MsrC) was investigated through comparative analysis of the wildtype (WT) *K. hansenii*, an *msrC*-deficient mutant (Δ*msrC*), and a complemented strain using the shuttle plasmid pUCD2. The Δ*msrC* mutation greatly affects growth, bacterial cellulose synthesis, abscisic acid response, quorum sensing and variability of cell size. Complementation restored some WT characteristics but revealed new phenotypes linked to bacterial cellulose synthesis. The tolerance to reactive oxygen species (ROS) was notably reduced in the absence of a functional MsrC. Additionally, the pUCD2 vector impacted pH and ROS tolerance. These findings highlight the multifaceted contribution of MsrC to bacterial physiology and biofilm dynamics, advancing our knowledge of its potential as a target for biofilm-related studies.

Keywords: *Komagataeibacter hansenii* (ATCC 23769); Free methionine-R-sulfoxide reductase (fRMsr / MsrC); reactive oxygen species (ROS); Phytohormones; Quorum sensing

AUTHOR'S DECLARATION

I hereby declare that this thesis consists of original work of which I have authored. This is a true copy of the thesis, including any required final revisions, as accepted by my examiners.

I authorize the University of Ontario Institute of Technology (Ontario Tech University) to lend this thesis to other institutions or individuals for the purpose of scholarly research. I further authorize the University of Ontario Institute of Technology (Ontario Tech University) to reproduce this thesis by photocopying or by other means, in total or in part, at the request of other institutions or individuals for the purpose of scholarly research. I understand that my thesis will be made electronically available to the public.

Rhys Bartlett

STATEMENT OF CONTRIBUTIONS

The method described in 2.5.3 was developed in part by the help of Nathanaël Bozor-Mbobi who helped gather preliminary data on *K. xylinus* leading to the interest in studying *K. hansenii* pH tolerance.

The results in 3.8 where obtained with the assistance of Maryam Ali who helped in the preparation of the experiment, running of the experiment and collection of data.

ACKNOWLEDGEMENTS

I would like to start by thanking my supervisor Dr. Janice Strap for her guidance. Thank you for your patience and reassurance despite my constant worrying and self doubt. I would also like to thank Dr. Dario Bonetta on my thesis committee for his suggestions to help improve the quality of my research as well as giving me access to his lab to use his equipment (large incubator, refrigerated centrifuge, and BioDrop DNA quantifier). I would like to thank Dr. Julia Green-Johnson for allowing me to use the plate reader in her lab.

I would like to thank my fiancée (at the time of writing) Kristal, for her support and encouraging me to pursue my master's degree. Thank you for enduring many home lectures to help me practice explaining what I'm learning and sharing my excitement.

I have learned a lot during my studies over the last two years in the Molecular Microbiology Biochemistry Laboratory that is not limited to just knowledge and techniques, but how to operate under pressure and develop a persevering work ethic. I will look back on these experiences with pride as both my launch point as a scientist and as a hallmark of personal growth.

TABLE OF CONTENTS

LIST OF TABLES

LIST OF FIGURES

ABBREVIATIONS AND SYMBOLS

ABA	abscisic acid
ACC	1-aminocyclopropanecarboxylate
ACP	acyl carrier protein
AHL	Acyl homoserine lactone
ATCC	American type culture collection
BLAST	Basic Local Alignment Search Tool
BC	bacterial cellulose
BCS	bacterial cellulose synthesis (protein)
bcs	bacterial cellulose synthesis (gene)
Δ	deletion
bp	base pair
CFU	colony forming unit
Cm	chloramphenicol
CmR	chloramphenicol resistance gene
DCF	2-7-dichlorodihydrofluorescein
DCFDA	2-7-dichlorodihydrofluorescein diacetate
DMSO	Dimethylsulfoxide

DNA	deoxyribonucleic acid
EDTA	Ethylenediaminetetraacetic acid
EPS	extracellular polysaccharide
fMet	free methionine
fRMsR	free methionine sulfoxide reductase
GAF	cyclic guanosine monophosphate-specific phosphodiesterases, adenylyl cyclases, formate hydrogenlyase transcriptional activator
gDNA	genomic deoxyribonucleic acid
IAA	indole-3-acetic acid
kb	kilobase pair
Kh	*Komagataeibacter hansenii*
Km	kanamycin
KO	Knockout
LB	Luria-Bertani (growth medium)
Met	methionine
Met-*R*-SO	methionine-*R*-sulfoxide
Met-*S*-SO	methionine-*S*-sulfoxide
Msr	methionine sulfoxide reductase

MW	molecular weight
MVC	mutant vector control
OD_{600}	optical density at 600 nm
PA	*Pseudomonas aeruginosa*
PCR	polymerase chain reaction
pMET	peptidyl methionine
QS	quorum sensing
ROS	reactive oxygen species
Rr	*Rhizobium radiobacter*
SAM	*S*-adenosylmethionine
SHF	Schramm-Hestrin + fructose growth media
SHG	Schramm-Hestrin + glucose growth media
Sp	spectinomycin
TAE	Tris-acetate-EDTA buffer
WT	wildtype
WVC	wildtype vector control
X-gal	5-Bromo-4-Chloro-3-Indolyl β-D-Galactopyranoside

Chapter 1. Introduction

1.1. Introduction to *Komagataeibacter*

Komagataeibacter spp. are gram-negative bacteria in the family Acetobacteraceae commonly found in nature on flowers and fruit. They are acetic acid bacteria that are able to oxidize ethanol into acetic acid, a process used in the production of many food products such as vinegar or kombucha tea (Cepec & Trček, 2022). Kombucha tea, a popular fermented beverage, is made by making a sugary tea and introducing a "scoby" (symbiotic culture of bacteria and yeast) which is a gelatinous pad housing the *Komagataeibacter* bacteria along with other fermenters such as yeast (Jayabalan *et. al*, 2014). Notably, the scoby is composed mainly of cellulose, an exopolysaccharide, produced by the *Komagataeibacter* bacteria synthesized at the air-liquid interface of its culture medium (Calderon-Toledo *et. al*, 2021).

Bacterial cellulose (BC) is composed of glucose molecules linked together to form long chains that associate together via hydrogen bonding. The chemical structure of BC is similar to that of plant cellulose, as both consist of glucose units linked by β-1,4-glycosidic bonds. However, purified BC differs in composition from plant cellulose in that it is not contaminated with hemicellulose and lignin which are vital components providing structural support for vascular plant growth and wood strength (Augimeri *et al.*, 2015). In *Komagataeibacter* spp., BC synthesis is facilitated by BcsA (bacterial cellulose synthase A), an inner membrane protein that contains a glycosyltransferase domain responsible for polymerizing cellulose chains from UDP-glucose monomers (Al-Janabi *et al.*, 2022; Wong *et al.,* 1990). The stability of BcsA depends on its interaction

with the periplasmic protein BcsB, and together, these proteins are indispensable for BC synthesis. Additionally, bacterial cellulose synthase C (BcsC) and bacterial cellulose synthase D (BcsD) play a role in exporting cellulose fibrils into the extracellular space via a proton antiporter accessing the proton gradient in the periplasmic space, ultimately leading to cellulose crystallization and pellicle formation (Al-Janabi *et al.*, 2022).

One intriguing aspect of *Komagataeibacter* biology is its sensitivity to various phytohormones, including ethylene, which has been found to impact the production of cellulosic pellicles, where the mass of pellicles increased after exposure to 10 μM ethylene supplied by etephon (Augimeri & Strap, 2015). This observation underscores the complex interplay between microbial physiology and external environmental factors.

1.2 Bacterial Biofilm Formation and Composition

Biofilms are a mode of growth utilized by numerous microorganisms to cope with a variety of environmental stressors. A biofilm is a structured community of microorganisms that adhere to surfaces and are encased in a self-produced matrix of extracellular polymeric substances. In contrast, a pellicle is a unique type of biofilm in that it is a floating mass of cells held together by a matrix of extracellular polymeric substances (Augimeri *et al.*, 2015). For *Komagataeibacter*, the synthesis of the pellicle is advantageous. The complex network of cellulose ribbons traps air, facilitating enhanced oxygen diffusion at the air-liquid interface. Additionally, it serves as a protective shield safeguarding the cells from desiccation and UV damage (Calderon-Toledo *et. al*, 2021).

In addition to extracellular polysaccharides, biofilms, including pellicles, often contain secreted enzymes or extracellular DNA that provide additional advantageous properties (Fleming & Wingender, 2010).

Extracellular enzymes present in certain biofilms can serve a diverse array of functions ranging from nutrition acquisition to defense against imposing competitors. Polysaccharide degrading enzymes can be used in both these applications and include: glycoside hydrolases, polysaccharide lyases and carbohydrate esterases. These enzymes act on polymeric saccharides and break them down into their monomeric components. This process has two key advantages: it frees up previously inaccessible sugars for use as carbon sources, and it weakens the biofilms of competing bacteria that use a different principal structural polysaccharide. The affected biofilm becomes more vulnerable and is at an increased risk of dissociating (Fleming & Wingender, 2010).

One common regulatory molecule conserved across diverse bacterial species for controlling biofilm production is cyclic di-GMP (c-di-GMP). This signaling molecule plays a pivotal role in modulating the transition between planktonic and biofilm lifestyles.

1.3 Bis-(3'-5')-Cyclic Dimeric Guanosine Monophosphate (c-di-GMP)

For a cell to coordinate a desired behaviour or survival response that might require multiple proteins to act synchronously, a unifying intracellular signal is needed. Once such signalling molecule is c-di-GMP.

In *K. xylinus,* it was first found that c-di-GMP binds to the pilZ domain located on the BcsA protein, serving as the signal for the cellulose synthetic complex of BcsA and BcsB to initiate polymerization of cellulose fibers (Weinhouse *et al.,* 1997).

Depending on the organism, c-di-GMP can stimulate different actions. For instance, in *Caulobacter crescentus*, a bacterium that switches between motile and sessile lifestyles, c-di-GMP acts as a messenger to signal the ejection of flagella, leading to a transition to the sessile state where it replicates to produce motile daughter cells (Paul *et al.*, 2004).

The structure of c-di-GMP consists of two guanosine monophosphate (GMP) molecules facing each other, with their phosphate groups connected. Its synthesis is mediated by diguanylate cyclases which remove two phosphate groups from two guanosine triphosphate (GTP) molecules and then bonds them together at carbon-3 to the oxygen of the adjacent phosphate group (Paul *et al.*, 2004). Conversely, the levels of c-di-GMP are regulated by phosphodiesterases by breaking down c-di-GMP into linear pGpG molecules (Ryjenkov *et al.*, 2005).

The precise control of cellular c-di-GMP levels is achieved through a delicate regulation of diguanylate cyclase and phosphodiesterase activity. This regulatory mechanism provides *K. xylinus* the means by which to adjust its BC biosynthetic system using this internal messenger molecule.

1.4 Quorum Sensing via *N*-acyl-homoserine Lactones

In order to coordinate the unified synthesis of a biofilm or any other survival behaviour, effective communication among cells is needed. Quorum sensing is the mechanism by which cells detect population density to determine appropriate responses to their environment. This communication relies on chemical signalling molecules referred to as autoinducers with one class of autoinducers being *N*-acyl-homoserine

lactones (AHLs) (Boukraa *et al.*,2011). The AHLs are composed of three main components which are the lactone moiety, a central amide and an acyl tail (Figure 1). Notably, the acyl tail is the main source of variability within AHLs; differences in the number of carbons in the tail or the presence of different side groups are used to differentiate these signalling molecules to increase the depth of communication between bacteria (Rodrigues *et al.*, 2022).

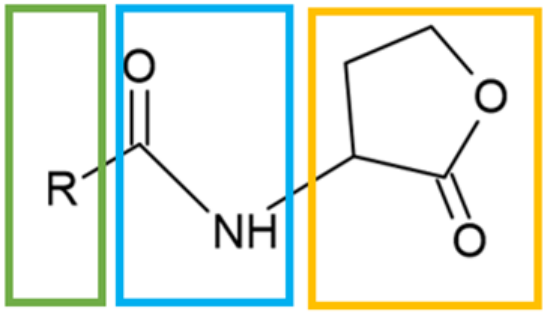

Figure 1. Chemical anatomy of an acyl homoserine lactone (AHL). The lactone moiety (yellow) is connected to the acyl R tail (green) by the amide linkage (blue).

The synthesis of AHLs (Figure 2) involves the combination of two precursor molecules facilitated by the LuxI protein, which is regulated by LuxR. The first precursor is an acyl group bound to acyl carrier proteins (ACP), where the acyl group becomes the acyl tail in the AHL. The length and composition of the acyl tail (R chain) can vary depending on the specific AHL being synthesized. The ketone group of the ACP-acyl forms half of the amide linkage which joins to the nitrogen of *S*-adenosylmethionine (SAM) (Ziesche *et al.*, 2018). After the AHLs are synthesized, they are exported into the extracellular environment where they are detected by surrounding cells to coordinate population behaviours.

The significance of AHLs for this thesis lies in their utilization of SAM, a methionine-derivative, in their synthesis.

Our interest in investigating AHLs stems from the question of whether the oxidation of free cellular methionine leads to decreased AHL production and by extension, quorum sensing in *K. hansenii*. In a study by Liu *et al.*, in 2019, it was experimentally determined that *Gluconacetobacter xylinum* (now renamed to *K. xylinus)* produces up to twelve different AHLs, each with varying lengths of carbon atoms in the R chain or possessing a secondary ketone group on carbon-2 of the R tail. When these AHLs were blocked by a quorum quenching protein, GqqA, it was observed that as the concentration of supplemented GqqA increased, the ability to form a pellicle decreased. This shows that quorum sensing plays a crucial role in pellicle formation in *K. xylinum*.

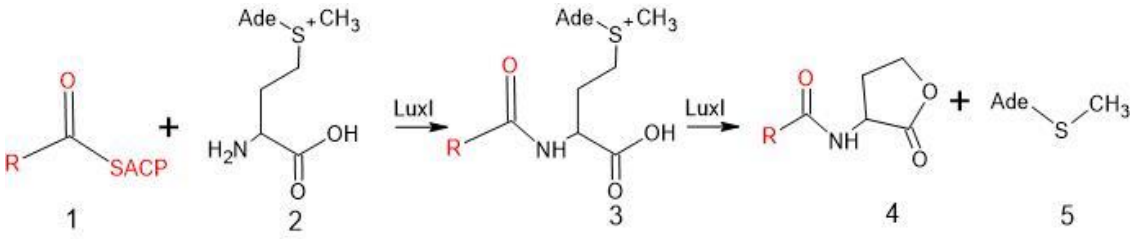

Figure 2. Synthesis of AHLs from methionine. The acyl group with the R chain ferried by ACP (1) and SAM (2) are joined by LuxI to make the acyl-SAM intermediate (3) which LuxI further converts to an AHL with an R group (4) and adenosine thioether (5) as end products.

1.5 Ethylene and Related Phytohormones

In plants, phytohormones serve as chemical messengers to coordinate various physiological responses and processes. One notable phytohormone, ethylene (Figure 3), a gaseous chemical with the formula C_2H_4, plays a pivotal role in initiating processes such

as seed germination, senescence and fruit ripening (Elias *et al*., 2017). The common sign of fruit ripening is the transition from a firm to a soft texture. This transformation occurs because ethylene stimulates the activity of hydrolases which break down starches into glucose, causing the fruit to soften and become sweeter (Lohani *et al.,* 2004). This process provides abundant glucose as a nutrient source for opportunistic plant-associated bacteria like *K. xylinus* enabling them to proliferate.

Another essential phytohormone is the auxin indole-3-acetic acid (IAA; Figure 3), which is responsible for coordinating cell elongation and division. IAA can induce stalk elongation or bending in vascular plants (Cruz *et al.,* 2023). IAA is a common plant-microbe communication molecule and is synthesized by many plant-related microbes including *Streptomyces* and *Rhizobium* (Kaur & Manhas, 2022). IAA and ethylene are functionally linked in regulating fruit ripening. Lohani *et al.* (2004) showed that in the Cavendish banana (*Musa acuminata),* the action of ethylene is halted, inhibiting fruit ripening and delaying release of simple sugars when exposed to IAA or the known ethylene action inhibitor 1-methylcyclopropene. Unlike some plant-associated bacteria, *K. xylinus* does not produce IAA, however, exogenously supplied IAA elicits increased growth rate and decreased pellicle formation (Qureshi *et. al,* 2013).

Abscisic acid (ABA; Figure 3) is a phytohormone that has been observed to amplify the effects of ethylene (Lohani *et al.,* 2004). It is used commonly as a response coordinator for stressful events like drought (Christmann *et al.,* 2007), extreme heat or cold, and hypersaline environments (Rabanni *et al.,* 2003). *K xylinus* has been found to synthesize ABA, and when exposed to exogenous ABA, it responds by increasing both

its growth rate and cellulose yield in pellicles (Qureshi *et al.*, 2013). It is not currently known whether *K. hansenii* produces ABA.

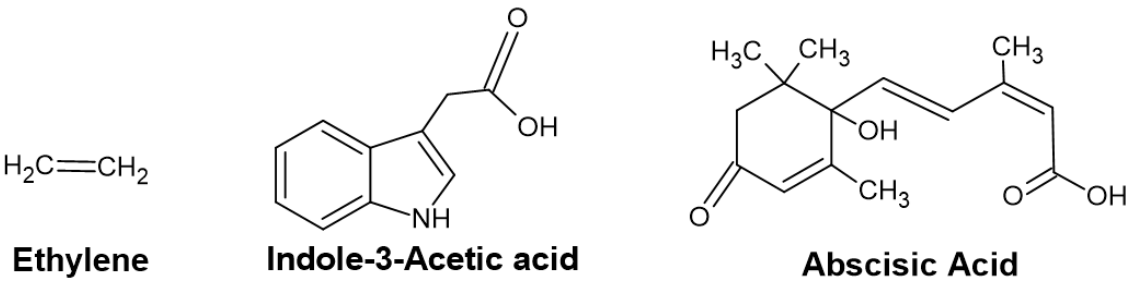

Figure 3. Chemical structures of the phytohormones ethylene, indole-3-acetic acid (IAA), and abscisic acid (ABA).

1.6 Plant Models of Ethylene Detection

Ethylene eliciting observable phenotypic responses from plants can be used as a means of gas detection when conventional measuring devices are not sensitive enough. One observable indicator of ethylene presence is the triple response phenotype in *Arabidopsis thaliana* sprouts. When *A. thaliana* seeds are incubated at room temperature (~23℃) in the absence of light, the presence of ethylene inhibits both root and hypocotyl growth, increases hypocotyl diameter, and causes a tightening of the apical hook (Guzmán & Ecker, 1990).

In *Arabidopsis thaliana,* there are five ethylene receptor isoforms; all operate with a similar mechanism of action: ETR1, ETR2, ERS1, ERS2 and EIN4. These receptors share common features, including a histidine or serine kinase domain, three N-terminal transmembrane domains, a GAF domain, and a copper ion binding domain which is believed to be the ethylene binding site (Binder, 2008; Lacey *et al.*, 2014).

Copper ions are used as a cofactor in many processes in aerobic respiration. In *A. thaliana,* copper ions are imported by the RAN-1 gene product. In *A. thaliana* RAN-1 mutants, ethylene binding specificity is affected, resulting in a reduced triple response phenotype upon exposure to trans-cyclooctene, a competitive ethylene receptor inhibitor. Supplementation of the growth medium with copper sulfate restores the triple response phenotype indicating copper ion deficiency leads to reduction in triple response phenotypes, and consequently, impaired ethylene detection. (Hirayama & Alonso, 2000).

According to the endosymbiotic theory of ethylene receptor acquisition, bacterial ethylene receptor candidates may possess a copper ion-containing domain or share a similar mechanism of action. This theory suggests that ethylene receptors were acquired in a manner analogous to the first chloroplasts as symbiotic bacteria (Lacey *et al.*, 2016).

Additionally, the GAF (cyclic GMP-specific phosphodiesterases, adenylate cyclases, and formate hydrogenlyase transcriptional activator (FhlA)) domain has been proposed as a potential protein binding site that may play a role in inhibiting the signaling capabilities of the ethylene receptor (Milić, *et al*. 2018).

1.7 GAF Domain

The GAF domain is also known as cyclic guanosine monophosphate-specific phosphodiesterases, adenylyl cyclases, formate hydrogenlyase transcriptional activator (GAF) domain, so named for its presence in various proteins involved in cyclic nucleotide signaling where it plays a role in binding to cyclic nucleotides like cGMP and cAMP, regulating various cellular processes. There have been many documented functions of the GAF domain in different proteins and in different organisms including

signal transduction, redox sensing (Kumar *et al.,* 2007), and light sensing (Su & Lagarias, 2007).

In plants, GAF domains have been found to be associated with chromophores, which are light receptors. Site-directed mutagenesis of a conserved tyrosine residue in the GAF domain of an *A. thaliana* phytochrome inhibits the plant's ability to sense light (Su & Lagarias, 2007). Analysis of absorbance spectra of chromophores with mutated tyrosine residues in the GAF domain show decreased light sensitivity where the best light sensitivity of a non-tyrosine residue in the GAF domain was Y276S at 34% compared to unmutated tyrosine residue. Interestingly, in other cases, the mutated phytochromes were turned fluorescent after a Y276H mutation (Fischer *et al.*,2005).

In bacterial models such as *Mycobacterium tuberculosis*, GAF domains have been shown to respond to environmental conditions relevant to aerobic respiration. The *M. tuberculosis* GAF domain of two different proteins, DosS and DosT, have unique sensing capabilities despite having greater than 70% conserved amino acid sequence and both using a heme group as cofactor. For example, the DosS protein was found to function as a redox sensor, detecting the oxidation state of iron in its heme cofactor. In contrast, the DosT protein increases its autokinase signalling activity in response to oxygen depletion using the oxygen binding properties of heme (Kumar *et al.,* 2007). This versatility underscores the capacity of the GAF domain to play multiple roles within a single protein, from intracellular cGMP signalling to actively detecting changes in the environment. Such adaptability is particularly important for strictly aerobic organisms that require oxygen for respiration and that continually generate reactive oxygen species.

At present, little is known about GAF-domain containing proteins in *Komagataeibacter* species.

1.8 Bacterial Responses to Ethylene

As mentioned above, the endosymbiotic theory attributes plants' ability to photosynthesize as resulting from an ancestral plant cell engulfing a photosynthetic cyanobacteria which later evolved into modern day chloroplasts. However, Lacey *et al.* in 2016 proposed that chloroplasts were not the only acquired trait during the endosymbiotic event but that it included certain proteins as well, specifically ethylene receptors. Using the bioinformatic search tool BLAST (Basic Local Alignment Search Tool), Lacey *et al.* identified similarities to known *Arabidopsis* ethylene receptor amino acid sequences in over 100 bacterial strains, including the cyanobacterium *Synechocystis sp.* PCC 6803.

The study further investigated the ETR1 homolog gene in *Synechocystis* (*SynEtr1*) by silencing it through gene disruption by insertion of a kanamycin resistance cassette. The resulting knockout (KO) mutant was then studied under ethylene exposure. Phototaxis assays were used to assess ethylene detection revealing that wildtype (WT) *Synechocystis* displayed increased positive phototaxis during ethylene exposure compared to air. Remarkably, the Δ*SynETR1* knockout exhibited an even more pronounced increase in phototaxis with more than triple the migrated distance observed in both air and ethylene conditions. The heightened phototaxis upon gene silencing suggests that ETR1 exerts an inhibitory effect on the ethylene phenotype.

Transcriptional analysis of *Synechocystis* exposed to 1 µL/L of ethylene or regular air showed the upregulation of 17 genes, 8 of which were either confirmed or predicted to

be involved in the production of extracellular polymeric substances (EPS) upon exposure to ethylene. EPSs play a crucial role in biofilm formation and the switch from a motile to sedentary state in bacteria (Lacey *et al*., 2018). *Komagataeibacter*, a non-motile bacterium, also produces EPS in the form of cellulose which can be used to evaluate its ethylene detection capabilities.

Augimeri and Strap (2015) showed that when *K. xylinus* was stimulated with ethylene, the *bcs* operon expression increased by nearly 1.5 times compared to *bcs* expression during growth without ethylene. The increase in *bcs* expression subsequently led to enhanced EPS production in the form of BC. It should be noted that among the hormones tested in that study, ethylene was unique in its ability to increase BC production without a proportional increase in bacterial growth, indicating that BC production and cell growth were asymmetrically affected when stimulated with ethylene.

1.9 Biosynthesis of Ethylene

Bacteria, including wildtype (WT) *K. xylinus*, have the potential ability to synthesize ethylene. Ethylene production by WT *K. xylinus* elicited a triple response phenotype from *A. thaliana* (Augimeri, 2016; Augimeri & Strap, 2015). It remains unknown whether *K. hansenii*, a related acetic acid bacterium, also produces ethylene.

In plants, ethylene synthesis occurs in a cyclical pathway known as the Yang cycle where methionine is converted to ethylene and secondary products from this process are metabolized to eventually regenerate methionine (Miyazaki & Yang, 1987). While it is uncertain if *K. xylinus* possesses the ability to regenerate methionine in this manner, preliminary BLAST searches for *A. thaliana* ethylene-forming homologs in *K.*

xylinus have identified homologs that can putatively convert methionine (MET) → (SAM)→ 1-aminocyclopropane carboxylate (ACC) → ethylene. This synthetic cycle, along with various other cellular processes, requires that methionine be in the proper chemical state in order for enzymatic reactions to proceed correctly. However, there are challenges for methionine to exist in the correct chemical state. One such challenge is the constant presence of reactive oxygen species.

1.10 Reactive Oxygen Species

A reactive oxygen species (ROS) refers to any oxygen-bearing molecule with the propensity to oxidize surrounding molecules to achieve a more favourable charged state. ROS are generated during oxygen-based metabolism due to the incomplete reduction of oxygen, which results in a net negative charge or unfavourable chemical state (Kappus & Sies, 1981). The work done by Imlay and Fridovich in 1991 showed that in *E. coli*, the major source of ROS, specifically superoxide (O_2^-), originates within the respiratory chain at the cytoplasmic membrane. They hypothesized that the production of superoxide was a consequence of electrons leaking through one of the proton pumps that use the passing of electrons to establish the proton gradient needed for ATP synthase function. It is this occasional electron leakage that converts dissolved O_2 into various ROS.

The formation of superoxide arises when a single electron reduces elemental oxygen to superoxide. Subsequent reductions can occur leading to the production of other ROS, such as hydrogen peroxide (H_2O_2) and hydroxyl radicals (OH^-). After one additional reduction of the hydroxyl radical, water is generated (Figure 4, Imlay, 2013). Before these ROS are converted to water, they pose an oxidative hazard to any molecule

in their vicinity, such as DNA, lipids and amino acids like methionine. It is worth noting that ROS can impact several pathways involving methionine and its metabolism in cells such as the transmethylation pathway (Ramachandran *et al.*, 2018), SAM biosynthesis (Kim *et al.*, 2006), and ethylene biosynthesis (Zhao *et al.*, 2023).

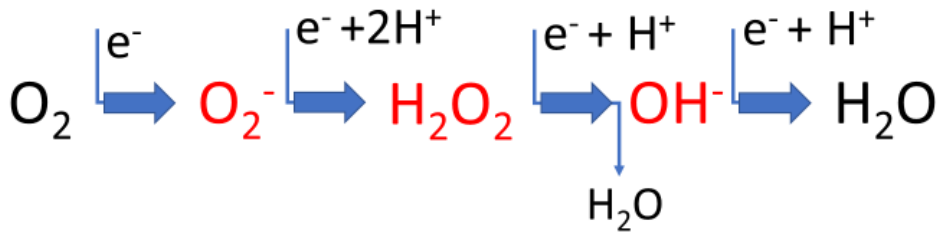

Figure 4. Conversion of reactive oxygen species. Superoxide (O2-) is reduced to hydrogen peroxide (H_2O_2) which is then further reduced to create water (H_2O) and a hydroxyl ion (OH-). After one final reduction step, water is produced. The molecules that are ROS in this pathway are labelled in red.

1.11 Methionine Sulfoxide Reductases

The amino acid methionine (Met) has an important role in protein synthesis in that it frequently serves as the first amino acid in polypeptide synthesis (Larsen *et al.*, 2005). If methionine undergoes undesired chemical alterations, protein synthesis can be negatively impacted to the detriment of the organism. One common modification that occurs is the oxidation of methionine into two diastereomers called methionine-*R*-sulfoxide (Met-*R*-SO) or methionine-*S*-sulfoxide (Met-*S*-SO). The distinction between these two diastereomers lies in the orientation of an extra oxygen atom around sulfur in the R chain of the amino acid (Figure 5) (Cheon & Gladyshev, 2011).

There are proteins that repair methionine that has been oxidized by reactive oxygen species (ROS); these are the methionine-sulfoxide reductases (Msr) and include MsrA, MsrB and free methionine-*R*-sulfoxide reductase (fRMsR) which will be referred to in this thesis as MsrC. Each of these Msrs have different specificities for the different states of methionine sulfoxide, which can exist as free methionine (fMet) when it is not bound to a protein, or peptidyl methionine (pMET) when it is bound. Both fMet and pMET can be in the *R* or *S* configuration. Notably, MsrC exclusively acts on fMet in the oxidized *R* diastereomer state (Le *et al.,* 2009).

The Msrs are able to correct methionine oxidation with the help of the protein thioredoxin which serves as the reducing agent (Figure 5). Thioredoxin contains two cysteine residues with exposed thiol groups which the Msrs use as the source of needed electrons and hydrogens to reduce the sulfoxide and eject the bound oxygen in the form of water. The thioredoxin forms a disulfide bridge from the oxidized thiol groups where it can then be regenerated by other reducing agents such as NADH (Lowther *et al.*, 2000).

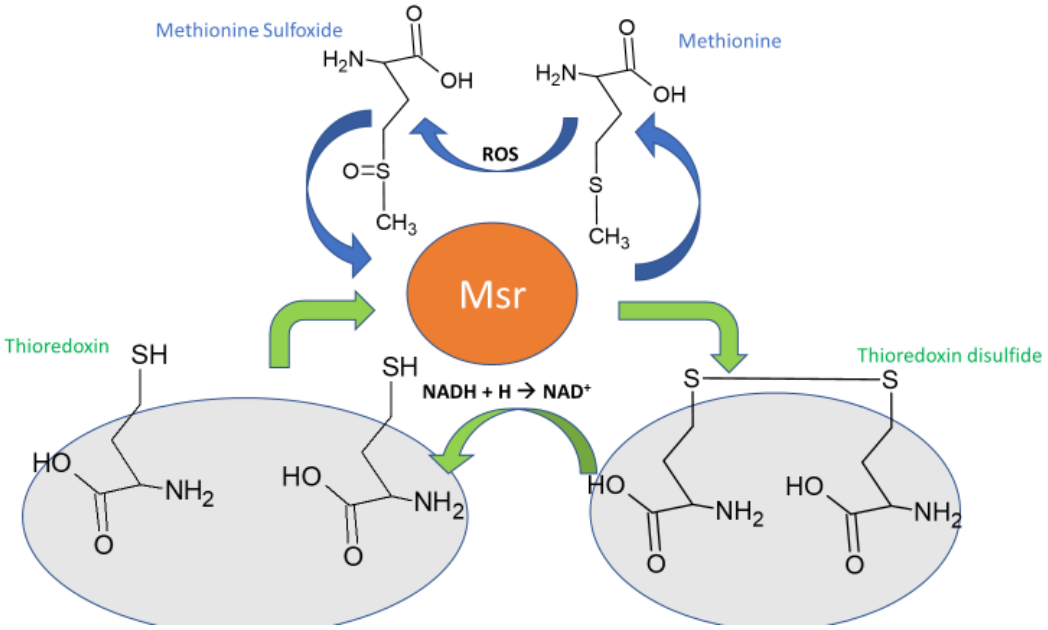

Figure 5. Reduction of methionine sulfoxide by action of the methionine sulfoxide reductases (Msr). ROS convert methionine to methionine sulfoxide, which is restored by the Msrs by using thioredoxin as a reducing agent. The two thiol groups of cysteine residues in thioredoxin are oxidized to create a disulfide bridge which is reduced by other agents in the cell such as nicotinamide dinucleotide (NADH) where it itself converts to NAD+.

The necessity of the Msrs can be observed when these genes are silenced, and the resulting mutants are exposed to oxidative stressors. For example, when exposed to increasing levels of H_2O_2, *Saccharomyces cerevisiae* becomes less tolerant to oxidative stress and its growth becomes partially or fully inhibited when any of the three Msrs are deleted. In the case of having both MsrA and MsrB silenced, resulting mutants had difficulty surviving the innate oxidative stress of metabolism without any additional exposure to oxidative stressors such as H_2O_2. This demonstrates that the innate ROS accumulation due to aerobic respiration has enough potency to adversely affect the survival of the host should the antioxidant systems be rendered non-functional (Le *et al.*, 2009).

Analysis into the structure of MsrC in *E. coli* reveals a GAF domain which is typically found in adenylyl cyclases or kinases involved in intracellular signaling. It has been postulated that the GAF domain in MsrC might be the binding site for Met-*R*-SO (Lin, *et al.,* 2007). In *K. hansenii,* homology modeling by Dr. Strap showed that the gene product of GXY_RSO3165, which was originally annotated as a GAF-domain containing protein, showed structural similarity to bacterial MsrC with a GAF domain. The GAF domain in MsrC raises the possibility that the protein may play a role in signal transduction, possibly by binding an as yet unidentified signal to regulate the reduction of methionine to impact methionine-based metabolic pathways such as ethylene, AHL, and protein synthesis; the GAF domain may also act a sensor for presence of ROS or O_2 by taking advantage of the propensity for methionine to oxidize, analogous to the heme group used in DosS and DosT in *M. tuberculosis* (Kumar *et al.,* 2007) described above. Further investigation is necessary to explore whether MsrC in *K. hansenii* plays a role in signal transduction pathways such as ethylene or ROS perception, which may be attributed to its possession of the GAF domain. At present, there is no literature documenting studies on Msrs within *Komagataeibacter* species.

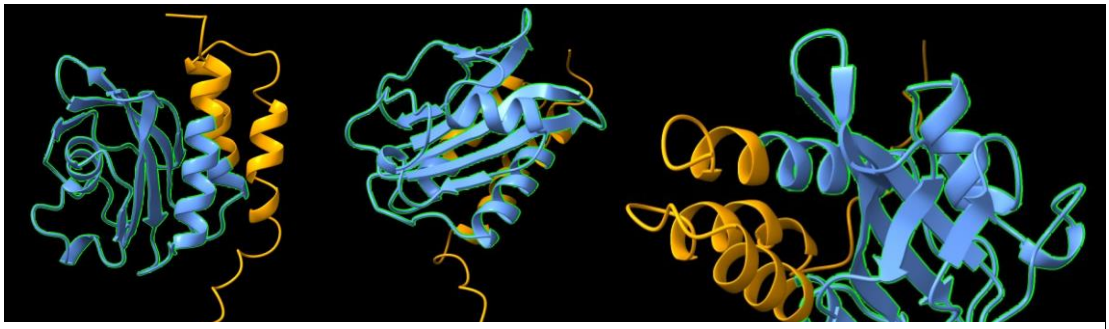

Figure 6. Three alternate views of GXY_RS03165 (MsrC) in *Komagataeibacter hansenii*. The GAF domain is visualized in blue. Protein Accession ID: WP_003617797.1. AlphaFold Protein Structure ID: AF-D5QC45. Visualized in ChimeraX version 1.6.1.

1.12 pH Tolerance

As the name implies, acetic acid bacteria live in acidic environments. There are two main strategies employed by these bacteria to mitigate the biochemical stress resulting from this low pH environment: proton-acetic acid antiporters and acetate oxidation (Xioman *et al.*, 2021).

In their study of the acetic acid resistance mechanism of *Acetobacter aceti*, Matsushita *et al.* (2005) deduced that there is a proton-acetic acid antiporter that exchanges intracellular acetic acid for extracellular protons. The second method of dealing with increasing concentrations of acetic acid levels involves acetate oxidation, where acetate ions combine with coenzyme-A in the citric acid cycle to consume the excess intracellular acetate (Saeki *et al.*, 1999). Elevated acetic acid concentrations also result in a high concentration of H^+ ions which can protonate various negatively charged molecules impeding their metabolic function. Acetic acid bacteria remedy this by leveraging the already established proton pumps which they use to maintain the proton gradient in their cell membranes for ATP synthesis and cellulose export.

Despite the established research on microbial defence mechanisms against acidic environments, the strategies employed by acetic acid bacteria to counteract more alkaline conditions, particularly those with pH levels exceeding their optimal homeostatic range is less understood. This thesis explores the possibility that the GAF-domain-containing protein, MsrC, may play a role in mitigating the effects of higher pH environments. As the environmental pH rises, there is an increase in the relative concentration of hydroxide ions (OH-) over hydrogen ions (H+), which can disrupt cellular processes.

The GAF domain, as mentioned above, is a widely recognized signalling motif, and proteins containing this domain are known to be involved in various cellular functions (Galperin, 2004). In acetic acid bacteria, which typically thrive at a pH of around 5, a GAF-domain-containing protein such as MsrC could contribute to pH homeostasis or tolerance through several potential mechanisms.

Firstly, it may serve as a pH sensor, detecting fluctuations in environmental pH and triggering signalling pathways that adjust the cellular proton concentration by either expelling H+ ions or facilitating their uptake, thereby maintaining a stable internal pH (Pardoux *et al.,* 2021; Soto *et al.,* 2018).

Secondly, the protein could regulate the activity or expression of ion transporters in the cell membrane, which are instrumental in balancing pH by moving ions in or out of the cell (Gamper *et al.,* 2007).

Thirdly, the GAF-domain protein might influence metabolic pathways to promote reactions that consume protons, thereby mitigating the effects of an alkaline shift, or to enhance acid production, helping to preserve the cell's acidic environment (Feehily & Karatzas, 2013).

Given the multifaceted nature of cellular pH regulation and the diverse functionality of GAF-domain-containing proteins, the potential dual role of MsrC in both ROS detoxification and adaptation to alkaline stress will be discussed further in this thesis.

1.13 GAF-Domain Containing MsrC in *K. hansenii*

GXY_RSO3165 (*msrC*) was identified through a bioinformatics screen of putative histidine kinases in the genome of *K. hansenii* ATCC 23769 (Strap, unpublished)*;* it was chosen for characterization due to the presence of a GAF domain. The *K. hansenii* ΔGXY_RSO3165 (Δ*msrC*) strain was previously created in the lab using PCR to amplify the upstream and downstream regions of the point of antibiotic resistance gene insertion within the *msrC* gene. The chloramphenicol (Cm) resistance gene was amplified from the plasmid pSEVA via PCR and ligated to these *msrC* end-fragments to create a strand of DNA that had the same 5' and 3' ends of the *msrC* gene but with the chloramphenicol resistance gene in-frame in the middle and an engineered stop codon replacing the 5' start codon of the gene; this is the *msrC* gene deletion construct (Figure 7). This deletion was then introduced into the WT *K. hansenii* and the construct was inserted into the genome by a double homologous recombination event.

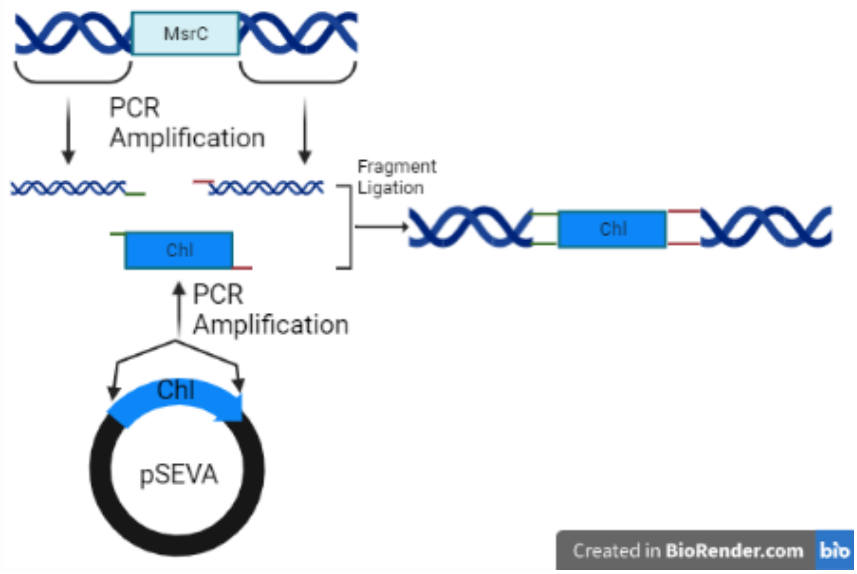

Figure 7. Creation of the *K. hansenii* Δ*msrC* mutation construct. PCR amplifications of upstream and downstream regions the native gene (*msrC*) are ligated to a chloramphenicol antibiotic resistance cassette (Chl) amplified from the pSEVA plasmid. Figure made using Biorender.com.

1.14 Objectives

The objectives of this thesis research were two-fold. Firstly, it aimed to complement the *K. hansenii* Δ*msrC* strain to investigate whether the complemented mutant behaviour aligns with that of the wild type, as previously explored in the dissertation by Jarret Arbing (2020). Additionally, the aim was to conduct an extensive characterization of the Δ*msrC* strain to elucidate the potential involvement of *K. hansenii* MsrC in ethylene reception, ROS tolerance, quorum sensing, growth rate, and pellicle formation. To address these objectives, various methodologies were used including assessing growth kinetics under phytohormone exposure (particularly ethylene), examining the tolerance to oxidative stress imposed by supplemented H_2O_2, quantifying

pellicle production and cellulose content, quantification of quorum sensing through detection of AHLs, and evaluating pH tolerance.

Chapter 2. Methodology

2.1 Bacterial Strains and Growth media

2.1.1 *Komagataeibacter hansenii*

Cultures of *K. hansenii* ATCC 23769 were grown in both agar plate and liquid culture using Schramm-Hestrin and glucose (SHG) medium. SHG is composed of 20 g/L glucose, 5 g/L peptone, 5 g/L yeast extract, 2.7 g/L sodium phosphate dibasic and 2.5 g/L citric acid dissolved in Milli-Q filtered water (Hestrin & Schramm, 1955). For agar plates, 15 g/L agar was added and the medium was sterilized in an autoclave at 121℃ for 20 minutes. For liquid cultures, 0.2 µM filter-sterilized cellulase (*Trichoderma reesei*, Sigma Aldrich) was added at 0.2% (v/v) concentration to prevent pellicle formation for homogenous turbidity. *Komagataeibacter hansenii* was streaked for isolated colonies from glycerol stock and incubated at 30℃. Liquid cultures were prepared in 5 mL SHG medium supplemented with filter-sterilized cellulase in screw capped culture tubes which were tilted at a 45^{o} angle. The tubes were incubated with agitation to allow for adequate mixing and aeration while preventing spillage. The cap of the culture tube was set loose to allow for air exchange promoting optimum growth. For larger-scale cultures, 5mL starter cultures were subcultured into a 50 mL screw capped tube containing 20 mL SHG. The screw cap of the 50 mL tube would be opened using aseptic technique at least once daily to allow for air exchange.

2.1.2 *Pseudomonas aeruginosa*

Pseudomonas aeruginosa was used as a positive control for quorum sensing assays. Cultures of *P. aeruginosa* were grown on Luria-Bertani (LB) plates or LB liquid media which were premixed and prepared according to the manufacturer's instructions (Bioshop Canada). *P. aeruginosa* was grown on LB agar plates at 37°C and in liquid LB media without agitation at the same temperature.

2.1.3 *Rhizobium radiobacter*

Rhizobium radiobacter (ATCC BAA-2240 (NTL4(pZLR4))) was used as a biosensor for AHL detection. Cultures of *R. radiobacter* were cultivated at 28℃ or 30℃ with agitation for liquid cultures. To maintain the plasmid NTL4(pZLR4), 15 µg/ml gentamicin (Gm) was added to LB plates or liquid AB minimal medium. AB medium growth media is made of 1 M stock salt solutions in water, filter sterilized with 0.2 µM filters and made to the following concentrations: 17.2 mM K_2HPO_4, 9.4 mM NaH_2PO_4, 18.6 mM NH_4Cl, 1.9 mM $MgSO_4$, 2 mM KCl, 90 µM $CaCl_2$ and 10 µM $FeSO_4$. A 20% (w/v) glucose solution in water was prepared, filter-sterilized with a 0.2 µm filter and added to a final concentration of 0.02% (v/v). All components of the AB media were purchased from BioShop Canada.

2.2 Creation of *K. hansenii* Mutants, Vector Controls and Complement

2.2.1 Preparation of Electrocompetent *Komagataeibacter hansenii* Cells

To prepare electrocompetent cells, starter cultures of *K. hansenii* and Δ*msrC* were inoculated using a single colony and grown until they reached an optical density (OD_{600}) within a range of 0.4-0.6. Once the cultures reached the desired OD_{600}, they were cooled

on ice for 10 minutes and were maintained on ice throughout the preparation process. Chilled cultures were transferred to centrifuge tubes and subjected to centrifugation at 3200 g for 12 minutes at 4℃, it should be noted that all centrifugation steps occurred at 4℃ for this procedure using a Sorvall ST 40R centrifuge. After centrifugation, the supernatant was carefully discarded, and the cell pellets were gently resuspended in an equal volume of chilled 1mM HEPES buffer. Subsequently, the cells were centrifuged again at 3200 g for 14 minutes. Once again, the supernatants were discarded, and the cells were resuspended in fresh 1 mM HEPES solution. A final centrifugation step at 1370g rpm for 14 minutes followed, with the resulting supernatant being discarded. The cells were resuspended in a 1/10 volume of ice-cold, sterile 15% (v/v) glycerol in water solution. The electrocompetent cells were stored in 50 µL aliquots at -80℃ until needed.

2.2.2 Electroporation Procedure for Complementation and Vector Control Creation

Plasmids were introduced into *K. hansenii* strains through electroporation. Aliquots of electrocompetent cells were thawed on ice and for each aliquot, the entire volume was transferred into a chilled 10 mm electroporation cuvette. To the volume of cells, 1 uL of 1/10 pUCD2::*msrC* in nuclease free water was added and mixed gently. Electroporation was conducted using a BTX- electroporator at 1850 Kv, followed immediately by the addition of 950 µL of prewarmed Super Optimal broth with Catabolite repression (SOC) medium (ThermoFisher Canada) into the cuvette. The entire cuvette volume was then transferred to a sterile centrifuge tube and incubated at 30℃ for *K. hansenii* electroporations and 37℃ for *E. coli* electroporations. Cells were allowed to recover for 24 hours for *K. hansenii* and 1 hour for *E. coli*. After the recovery period,

liquid cultures were spread onto agar plates supplemented with 50 µg/ml kanamycin (Km) for *E. coli* or 250 µg/mL spectinomycin (Sp) for *K. hansenii*.

2.2.3 Creation of *K. hansenii* Δ*msrC* Complement Strain

To complement the *ΔmsrC* mutant, PCR primers were designed for the 5' and 3' untranslated regions (UTR) flanking the *msrC* gene in the WT *K. hansenii* genome (Table 1). The genomic DNA (gDNA) was extracted from WT *K. hansenii* using the Biobasic genomic DNA kit (BS353) following the manufacturer's instructions. The endogenous *msrC* gene was amplified by PCR and confirmed via gel electrophoresis. The PCR was carried out using the following program: 1 cycle of 98^{o}C for 30 seconds, 30 cycles of the following steps: 98^{o}C for 8 seconds, and 69^{o}C for 30 seconds, the last step was one cycle of 72^{o}C for 120 seconds. The resulting PCR products were purified using the EZ-10 Spin Column PCR Products Purification Kit (Biobasic, BS363), and quantified using the Biodrop DUO.

The shuttle vector used to carry the WT version of the *msrC* gene insert was pUCD2 (ATCC 37342), a 13 Kb plasmid that has resistance genes for tetracycline (Tet), kanamycin (Km) and spectinomycin (Sp) as well as ori 322 which is compatible with the *K. hansenii* DNA translation system. Purified pUCD2 was linearized by *PstI* (NEB R0140S) digestion. Subsequently, both the linearized plasmid and the purified *msrC* gene insert were independently blunt-ended using the NEB Quick Blunting Kit (E1201S). Then, using the NEB Quick Ligation Kit (M2200S), the gene insert and plasmid were mixed in a 3:1 insert:vector molar ratio and ligated together as per instructions from the manufacturer, creating the complementation construct pUCD2::*msrC* (Figure 8).

The complementation construct was introduced into electrocompetent *E. coli* DH5α following the procedure outlined in 2.2.3. Plasmid selection was performed on LB agar plates containing 50 µg/ml kanamycin (LBKM50). A patch plate of *E. coli* transformants putatively containing pUCD2::*msrC* was made on a fresh LBKM50 agar plate. To verify the presence of the *msrC* insert, plasmids from the transformants were extracted using a Biobasic EZ-10 spin column plasmid DNA miniprep kit designed for low copy plasmids (BS4139). Subsequently, the purified plasmids were used as templates for PCR using the same primers that were used for the initial amplification of *msrC* from WT *K. hansenii*, KhMsrC-EcoRV Forward and KhMsrC-PstI Reverse (Table 1).

One of the recombinant plasmids that tested positive for the insert and which showed no sign of concatenation was then introduced into electrocompetent Δ*msrC* (prepared according to 2.2.2) and selected on SHGCm500Sp250. Electroporants were patch-plated and screened via PCR using plasmid DNA as template. Agarose gels were made to 1.0% (w/v) in tris-acetate-EDTA (TAE) buffer. The gels were electrophoresed with 100V and visualized with either 10 µM ethidium bromide in water and UV illumination or SafeStain and visualized on a blue light transilluminator. Complementation of the Δ*msrC* mutation was confirmed by sequencing the resulting amplicons.

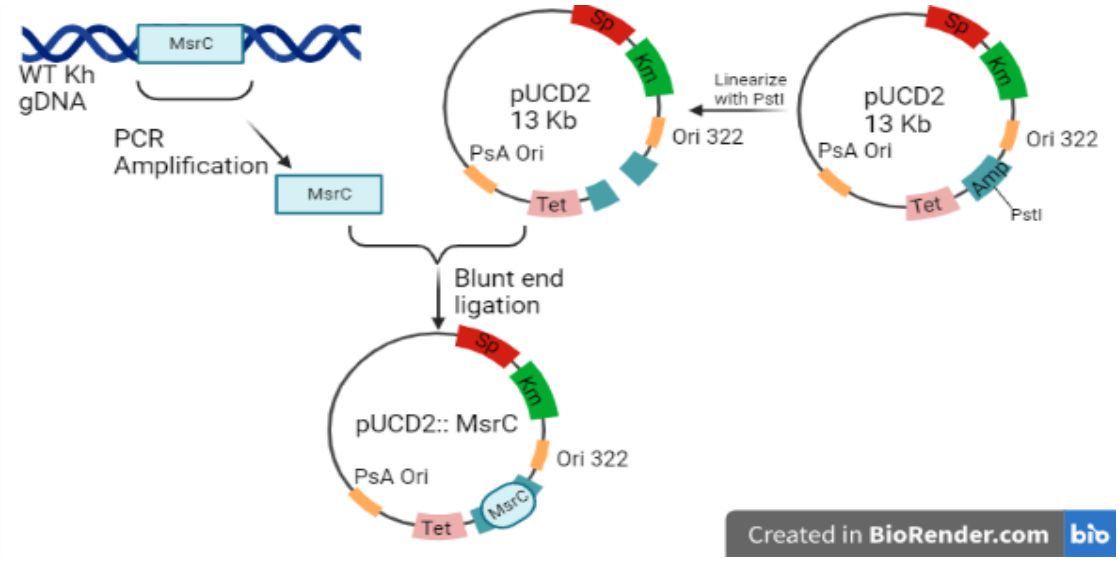

Figure 8. Creation of pUCD2::*msrC* complementation construct. The native gene (*msrC*) and its 5' and 3' UTR were amplified by PCR. The shuttle vector pUCD2 was linearized by *PstI* restriction enzyme digestion. The *msrC* amplicon and linearized pUCD2 were ligated by blunt-end ligation to create the pUCD2::*msrC* complementation construct. Figure was made using Biorender.com.

2.2.4 Complementation Primers

For the thesis, only one primer pair was used for PCR (Table 1), it was to amplify the *msrC* region in *K. hansenii* gDNA and to detect the presence of the complementation insert within pUCD2.

Table 1. Primers used for amplification of *msrC* from WT *K. hansenii*.

Primer	Sequence (5' → 3')	Tm (°C)	Expected Amplicon Length (bp)
KhMsrC-EcoRV Forward	TTCGGTCCTCGATATCCCGGGCCTCC TGCCTTG	62	712
KhMsrC-PstI Reverse	TTCGGTCCTCCTGCAGGGACAGTTC ATTTCCAGAAAAACGA	60	

2.2.5 Creation of Empty Vector *K. hansenii* Control Strains

In addition to the complemented strain, two control strains were generated: wildtype vector control (WVC) and mutant vector control (MVC). The WVC is WT *K.*

hansenii transformed with empty pUCD2; it was selected for on SHGSp250. The MVC is Δ*msrC* transformed with empty pUCD2; selected for on SHGCm500Sp250.

To confirm insertion of the pUCD2 plasmid, cultures of both control strains had their plasmids extracted using the Biobasic EZ-10 spin column plasmid DNA miniprep kit designed for low copy plasmids (BS4139). These extractions were analyzed using an agarose gel and compared to the WT *K. hansenii* for any observable banding present in the WVC and MVC that is absent in the WT indicating pUCD2 has been successfully inserted.

2.2.6 Strain Coding for Quality Control

To ensure that cross-contamination of strains did not occur, liquid cultures of the five strains (WT, Δ*msrC*, WVC, MVC, and complement) would be occasionally subjected to a strain coding test to affirm each strain was growing as expected. The strain coding test was done by inoculating liquid SHG medium along with SHGCm500, SHGSp250 and SHGAmp500 with the same volume of inoculum of test culture at the same time and incubated at 30℃ for 3 days or until growth was observed. A schematic of the quality control assay is shown as a truth table used to confirm strain identity (Figure 9).

Figure 9. Truth table for strain coding to ensure quality control of the five *Komagataeibacter hansenii* strains (WT, Δ*msrC*, WVC, MVC, and complement). The three testing antibiotic conditions were 500 µg/mL chloramphenicol (Cm500), 250 µg/mL spectinomycin (Sp250), and 500 µg/mL ampicillin (Amp500).

2.3 Minimum Inhibitory Concentration

To ascertain the appropriate level of spectinomycin required for selection and maintenance of pUCD2 in *K. hansenii*, a minimum inhibitory concentration (MIC) assay was performed on both WT and Δ*msrC*. Concentrations of spectinomycin were tested at the following concentrations in µg/ml: 1000, 800, 640, 512, 409, 327, 261, 208, 166, and 134. Wells of a 96-well plate were inoculated to final OD_{600} of 0.05 of both WT and Δ*msrC* and allowed to incubate for several days at 30°C, with three biological replicates and one technical replicate (Figure 10A).

2.4 Pellicle Assay

To assess cellulose production differences among strains, a pellicle assay was performed. The five strains (WT, Δ*msrC*, WVC, MVC, and complement) were grown in SHG medium with 0.2% (v/v) cellulase until mid-log phase (0.4-0.6 OD_{600}). The inoculum was then split into two aliquots. Both aliquots were centrifuged at 10,000 rpm. Once cells were pelleted, the supernatant was removed and the pellets were washed with sterile MQH_2O and to ensure no cellulase carried over from the initial culture. Each aliquot of culture was then adjusted to OD_{600} 0.5 in either SHG or SHF. The standardized inoculum was used to inoculate 24-well microplates containing either SHG or SHF to a final volume of 2 mL and a starting OD_{600} of 0.05. The plates were left to grow statically at 30^{o}C for 14 days.

Following the 14-day growth period, the pellicles were subjected to a treatment process to eliminate the bacteria and remove cellular debris to prevent them from affecting cellulose yield. The pellicles were transferred into pre-weighed 2 mL microcentrifuge tubes and treated with 1 mL of 1 M NaOH at 80^{o}C for 1 hour, after which the liquid was removed and replaced with the same volume of NaOH and left at 50^{o}C overnight. The following day, the pellicles were washed repeatedly with sterile MQH_2O until at least 6 random samples showed neutral pH using litmus paper. If any one sample showed a pH above 7, the entire sample set would be subjected to an additional wash step. Once neutrality was reached, the sample tubes were left open to dry in a drying oven at 60^{o}C for at minimum 2 weeks.

After drying, samples were then re-evaluated using the same analytical balance used for the initial weights of the empty tubes and difference in mass was calculated and recorded.

2.4.1 Anthrone Assay

Since cellulose is a glucose polymer, the cellulose content of the processed pellicles were quantified using the anthrone assay. The anthrone assay estimates cellulose content indirectly by measuring the glucose released upon its hydrolysis (Gurgel *et al.,* 2012). When the cellulose is mixed with sulfuric acid, it undergoes hydrolysis, releasing glucose to form hydroxymethyl furfural which has a yellow colour. The hydroxymethyl furfural then reacts with the anthrone in solution forming a complex that turns the mixture from a pale yellow to deep green colour (Chu *et al.,* 2018). The intensity of the green colour is proportional to the concentration of hydroxymethyl furfural which correlates with the amount of glucose released from cellulose during hydrolysis. The anthrone was prepared as a 0.2 % (w/v) solution in 96% sulfuric acid. The processed pellicles were first immersed in 500 µL of sterile MQH_2O and vortexed to ensure the pellicle was suspended freely within the water. To each sample, 1 mL of sulfuric acid was carefully added followed by incubation at 100^{o}C for 20 minutes in the fume hood, resulting in the formation of a solution containing hydrolyzed cellulose which had a deep black colour. The hydrolyzed samples were then diluted in 0.2% (w/v) anthrone in sulfuric acid solution using a ratio of 3:47 repeating the 20-minute 100^{o}C heating step, leading to a green colour. The A_{620} of each sample was measured and compared to a standard curve created with known concentrations of glucose ranging from 0 µg/ml to 100 µg/ml. The A_{620} values of the diluted samples were determined and the original concentration of cellulose in each sample was calculated from the standard curve, dividing by the dilution factor and expressed as glucose equivalence in milligrams.

2.5 pH Tolerance Assay

2.5.1 pH Adjusted SHG Medium

To investigate whether MsrC plays a role in pH tolerance in liquid cultures, SHG was prepared so that the final pH ranged from 4 to 7. To adjust the pH to 4, 1 M HCl was used, whereas 1 M NaOH was used to adjust the pH of SHG between pH 5.5 - 7. The acidified media was autoclaved at 120^{o}C for 20 minutes. The pH of the acidified media was recorded before and after sterilization to ensure that the heat did not alter the pH. SHG media between pH 5 - 7 were filter-sterilized using Nalgene 115-mL filter units. It should be noted that SHG has a pH of 5.2.

2.5.2 pH Tolerance of *Komagataeibacter hansenii* Cultures

The five strains (WT, Δ*msrC*, WVC, MVC, and pUCD2::*msrC*) were grown in SHG to an OD_{600} of 0.4-0.6 and adjusted to an OD_{600} of 0.5 for the inocula. In a 96-well plate, SHG from pH 4 - 7 and unaltered pH SHG (pH 5.2) were dispensed and inoculated to a final OD_{600} of 0.05. Each media had a sterile control included with 3 biological replicates and 3 technical replicates. The plates were grown statically at 30^{o}C for 5 days, and every 24 hours the plate would be agitated for one hour at 30^{o}C at 300 rpm and the OD_{600} recorded.

2.5.3 Survivability of *Komagataeibacter hansenii* After Exposure to Non-Standard pH

The impact of pH on the viability of the five strains (WT, Δ*msrC*, WVC, MVC and complement) was evaluated by exposure to the pH-adjusted media and comparing the colony forming units (CFUs) to those observed for the standard SHG medium. The *K.*

hansenii strains were grown with 3 biological replicates and standardized to OD_{600} of 0.5. The cultures were tested at four different pH conditions in SHG: unaltered at pH 5.2, as well as pH 4, 5, and 7. The inoculum was added in the pH-adjusted media to a final OD_{600} of 0.05 and incubated at 30^{o}C with agitation for one hour.

After the incubation period, the cultures were serially diluted 10-fold and 5 µL from each dilution was spotted onto SHG plates. The plates were incubated at 30^{o}C until isolated colonies were visible and countable. Representative pictures of the dilutions were reported. Isolated colonies were counted and using the known dilution of the spot, the CFU/ mL was calculated to determine the amount of viable cells present in the originally undiluted sample post-exposure and compared to the SHG (pH 5.2) to obtain the % survival.

2.5.4 Comparison of *K. hansenii* / pUCD2 (WVC) Transformants to Confirm Accurate Representation

Observable differences between the WT and WVC strains in the experiment described in 2.5.2 raised questions about how representative the specific WVC transformant tested actually was. From the data, it was unclear whether the observed differences were due to transformation-related effects or whether they were a true reflection of the *K. hansenii*/pUCD2 phenotype. To determine whether the WVC results were characteristic of the strain or merely artifacts of that particular transformant, two additional transformants, derived from the same electroporation event as the original WVC strain, were cultivated. These two transformants were subjected to the experiment described in 2.5.2 and compared to the data for the initial WVC transformant to

determine if all three transformants behave similarly or if there are individualistic effects taking place.

2.6 Growth Kinetics

The effects of phytohormones, oxidative stress and pH on the growth of the *K. hansenii* strains (WT, Δ*msrC,* WVC, MVC and complement) were analyzed to determine the impact of the Δ*msrC* mutation, the pUCD2 plasmid, and the pUCD2::*msrC* complementation construct. This was done with a BioScreenC plate reader which incubates up to two 100-well honeycomb plates at 30^{o}C with constant agitation. The strains were grown to OD_{600} 0.4 - 0.6 and adjusted to OD_{600} 0.5. Conditions tested were unaltered SHG (pH 5.2), 10 µM IAA, 10 µM ABA, 1 mM ethylene, 10 µM hydrogen peroxide as well as SHG at pH 4 ,5, 6, and 7. A sterile control was included for each media type. Inoculations were done to a final OD_{600} of 0.05 and 0.2% cellulase. The growth period was 7 days with OD_{600} readings taken every 3 hours.

2.7 Cellular Morphology

To determine whether the changes made to the media as described in section 2.6 affected the physical characteristics of the cells, 10 µL from one representative well of each media type and strain (as in section 2.6) was taken at the end of the growth experiment and used to prepare a wet mount on glass microscope slides. The slides were observed under 1000x magnification using dark field microscopy to look for any changes to the morphology of the cells, including the cell shape and length. Random fields of view were photographed and the bacteria were measured until 50 - 100 measurements were obtained.

The lengths of cells were quantified using ImageJ software (Schneider *et al.*, 2012). Prior to analysis, photographs were optimized for contrast to enhance feature definition. The 'Threshold' function in ImageJ was applied to retain the majority of cells while excluding background noise and light variations. Calibration of the internal scale was performed using a reference photo of a 10 μm scale. The 'Analyze Particles' feature of ImageJ was used to automatically determine the cell lengths. The analysis utilized the Feret diameter, a geometric measure that calculates the longest distance between any two points along the cell boundary in μm. ImageJ draws tangent lines along the cell outline and computes the longest distance between any two parallel tangent lines that are the farthest apart from each other. This way the longest straight line that passes through the cell can be determined automatically, allowing for high throughput measuring of cell lengths.

2.8 Reactive Oxygen Species Assay

To determine the role of MsrC as a potential redox sensor in *K. hansenii*, the ROS levels present in live *K. hansenii* cells under both homeostatic and exogenous ROS-exposed conditions were analyzed using the oxidation sensitive fluorophore 2-7-dichlorodihydrofluorescein diacetate (DCFDA). The DCFDA (Sigma Aldrich) was prepared in dimethylsulfoxide and added to aliquots of bacterial culture to a final concentration of 10 μM. The culture aliquots with DCFDA were allowed to incubate for 30 minutes at 30^{O}C with agitation in the dark. The dye only becomes fluorescent after entering live cells where cellular esterases remove the acetate groups from DCFDA to produce dichlorofluorescein (DCF). Once the DCF conversion treatment was completed,

95 µL of treated cells were added to wells in a black UV transparent clear bottom 96-well plate. This was done with three biological replicates of each of the *K. hansenii* strains with three technical replicates. Two different conditions were observed concurrently, one would be measured without exogenously added hydrogen peroxide to obtain the homeostatic level of ROS. A second set of cells from the same cultures were treated with hydrogen peroxide to a final concentration of 1 mM. Fluorescence was measured with an excitation wavelength of 475 nm and emission wavelength of 525 nm.

The observation period lasted 30 minutes with fluorescence readings taken every 5 minutes using a Cytation 5 plate reader (BioTek). The change in fluorescence over time was compared between the five *K. hansenii* strains (WT, Δ*msrC*, WVC, MVC, and complement). Additionally, the fluorescence of the hydrogen peroxide-exposed cells and the untreated cells were compared at the 30-minute time point.

2.8.1 Cell viability After Controlled ROS Exposure

To evaluate the lethality of ROS, the five strains (WT, Δ*msrC*, WVC, MVC and complement) were subjected to increasing levels of exogenous hydrogen peroxide and then 10-fold dilutions were spot-plated to determine the survivability compared to the control of no additional hydrogen peroxide. The strains were grown in 3 biological replicates and standardized to OD_{600} of 0.5. The cultures were tested at four different concentrations of hydrogen peroxide each with three technical replicates: 1mM, 3 mM and 5 mM with a negative control of 0 mM (no added hydrogen peroxide).

After the hydrogen peroxide was added, the cultures were incubated at 30^{o}C with agitation for 30 minutes. The cultures were then spotted according to the protocol

described in 2.5.3. Representative pictures of the dilutions were reported. Dilutions containing isolated colonies were counted and using the known dilution of the spot, the CFU/ mL was calculated and compared to the 0 mM control to obtain the % survivability.

2.9 Evaluating Production of Extracellular AHLs in *Komagataeibacter* Strains Using the Biosensor *Rhizobium radiobacter*

To investigate whether MsrC plays a role in quorum sensing, the presence of extracellular AHLs were measured from the supernatants of the five *K. hansenii* strains (WT, Δ*msrC*, WVC, MVC, and complement) were collected from cultures grown to mid-log growth (OD_{600} 0.4 - 0.6); this was done with three biological replicates in SHG (pH 5.2). The biosensor *Rhizobium radiobacter* has the plasmid pZLR4 that consists of two components: *luxR* and *lacZ.* The *luxR* gene encodes a transcriptional activator protein, LuxR which binds AHL molecules. The *lacZ* gene encodes the β-galactosidase enzyme that can cleave the substrate 5-bromo-4-chloro-3-indolyl-β-D-galactoside (X-gal) to produce a blue coloured product (Puelles *et al.,* 2021). In the absence of exogenous AHLs, LuxR produced by the *luxR* gene remains inactive and cannot bind to the promoter region of the *lacZ* gene, so β-galactosidase is not produced and the X-gal remains intact. When exogenous AHLs are present, they can diffuse into the *R. radiobacter* NTL4(pZLR4) cells. If the AHL molecules match the specificity of the LuxR, the LuxR becomes activated by binding to the AHL. Once LuxR binds to AHL, the LuxR-AHL complex can activate transcription of the *lacZ* gene by binding its promoter region leading to the production of β-galactosidase, which cleaves X-gal into a blue-colored product. The intensity of the blue color is directly proportional to the concentration of exogenous AHLs (Paldrychová *et al.,* 2019; Prakash Singh & Greenstein, 2006).

The *R. radiobacter* was grown to OD_{600} 0.4 - 0.6 according to the growth conditions listed in 2.1.3 and adjusted to OD_{600} 0.2 by diluting with fresh ABGm15. In a 96-well plate, 50 µL of adjusted *R. radiobacter* was added to 15 µL of supernatant from each strain at the same growth stage; this was done with four technical replicates. The negative control for this experiment was the addition of 15 µL sterile water instead of supernatant to the *R. radiobacter*. The plate was incubated at 28°C with shaking agitation for 18-24 hours. At the end of the growth period, an equal volume of lysis buffer was added containing 0.02% (w/v) cetrimonium bromide, 4.3 mg/mL $MgCl_2$ - 6 H_2O, 14.1 mg/mL Na_2HPO_4 - 7H_2O, 2.3 mg/mL NaH_2PO_4 - H_2O and 80 µg/mL X-gal. All ingredients for the lysis buffer were obtained from BioShop Canada. Lysis was allowed to proceed for 24 hours at room temperature with agitation.

The appearance of the blue indicator caused by the LacZ protein acting on the X-gal was quantified by taking the A_{615} and A_{660} of the wells using a Cytation 5 plate reader. Beta-galactosidase induction was calculated by dividing the values obtained for each of the *K. hansenii* supernatants by those obtained from the untreated control.

2.9.1 Impact of Supernatant Carryover of Chloramphenicol and Spectinomycin on Biosensing Capability of *R. radiobacter*

Due to the presence of antibiotics in the growth media in four of the five strains tested (Δ*msrC*, WVC, MVC and complement), it was investigated whether the antibiotics introduced to the biosensor through the supernatants would lead to a decrease in the sensitivity of *R. radiobacter* to detect AHLs. To account for the different supernatants which contain Cm, Sp, or both, a *R. radiobacter* culture was prepared as mentioned in

section 2.9 then split into four aliquots, each with different combinations of additional antibiotics so that all tested supernatants had the same levels of Cm and Sp. One was left unaltered (AB GM15) to be used on the MVC and complement strain. The second was AB Gm15Cm115 for the WVC, the third was AB Gm15Sp58 for the Δ*msrC* mutant, and finally, AB Gm15Cm115Sp58 was used for the WT supernatants. A positive control of *P. aeruginosa* supernatant was used with the additional antibiotics (AB Gm15Cm115Sp58) and data was collected and analyzed in the same manner described in section 2.9

2.9.2 Evaluating Production of Extracellular AHLs Using *Komagataeibacter* Supernatants Grown in the Absence of Antibiotics

To observe the amount of extracellular AHLs produced by the five strains (WT, Δ*msrC*, WVC, MVC and complement) without the impedance of added Cm or Sp, supernatants were prepared according to section 2.9 except for the exclusion of Cm or Sp to the cultures. The rest of the procedure and analysis of 2.9 was repeated.

After harvesting the supernatants, the antibiotic resistant strains were streaked onto SHG plates containing their respective selective antibiotics with MVC and complement on SHGCm500Sp250, WVC on SHGSp250 and Δ*msrC* on SHGCm500 to ensure that the pUCD2 plasmids, the pUCD2::*msrC* construct, or the Δ*msrC* mutation were not lost over the culturing period from lack of antibiotic selection.

Chapter 3. Results

3.1 Minimum Inhibitory Concentration Assay

All tested concentrations of spectinomycin from 1000 µg/mL to 134 µg/mL in both the WT *K. hansenii* and the Δ*msrC* mutant showed inhibition of growth compared to

the positive control with no antibiotics (Figure 10). In the event that the selecting concentration for the pUCD2 plasmid is near the 134 µg/mL determined by the MIC assay, the concentration of spectinomycin used to culture plasmid-bearing cultures was 250 µg/mL. The rationale for this decision was to provide extra assurance that in the event of antibiotic degradation by natural decay or by (in)direct action of the bacteria, sufficient antibiotics should remain during long culture periods (such as the 14-day growth time for the pellicle assay mentioned in 2.4) to ensure that plasmid-containing cultures were selected. No observable differences in growth inhibition were observed between the addition or exclusion of 0.2% (v/v) cellulase.

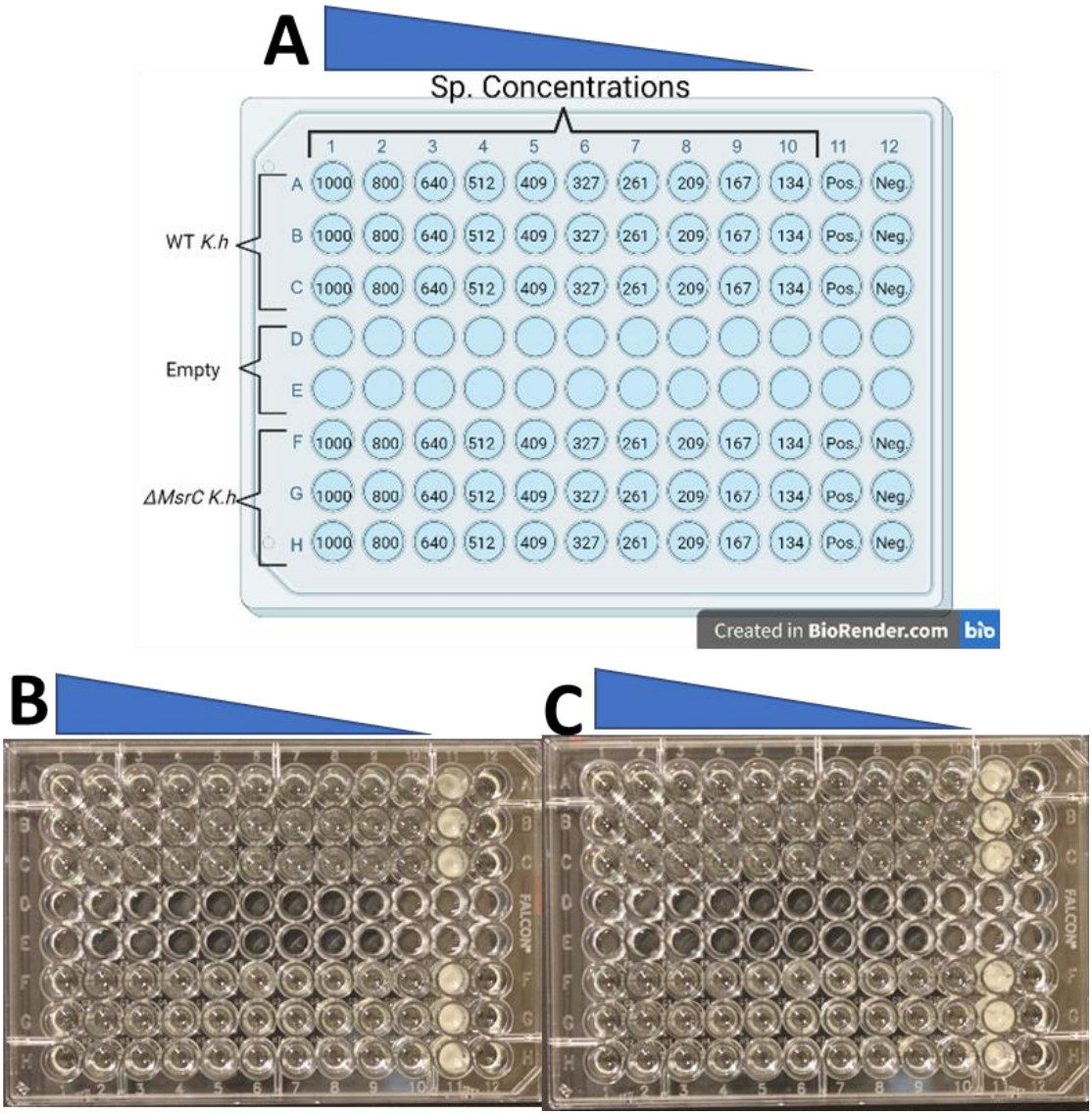

Figure 10. Minimum inhibitory concentration (MIC) assay for spectinomycin WT *Komagataeibacter hansenii* and *ΔmsrC*. Diagram depicting the well layout of the MIC assay, listing concentration of spectinomycin, the positive untreated control (Pos) and negative sterile control (Neg) (A). Impact of spectinomycin on *K. hansenii* without 0.2% (v/v) cellulase (B) and with 0.2% cellulase (v/v) added (C).

3.2 Creation and Validation of Complement Strain

To confirm the successful creation of the complementation strain, PCR amplification was conducted using pUCD2::*msrC* as template DNA. This amplification yielded two distinct products, one approximately 1500 bp and the other ~700 bp as shown

in Figure 11. Sequence analysis revealed that the 1500 bp band shared similarity with the *CmR* region in the *ΔmsrC* mutant (Figure 11A), while the ~700 bp amplicon aligned closely to the *msrC* gene (GXY_RS03165; Figure 11B). This indicates that within the complementation strain, the original disruption caused by the *CmR* cassette is coexisting with the pUCD2::*msrC* complementation construct. Amplification of the *CmR* cassette further suggests that the plasmid preparation contained residual genomic DNA. Having established successful complementation, this strain was cultivated for further comparative analysis with the other *K. hansenii* strains (WT, Δ*msrC*, WVC, and MVC).

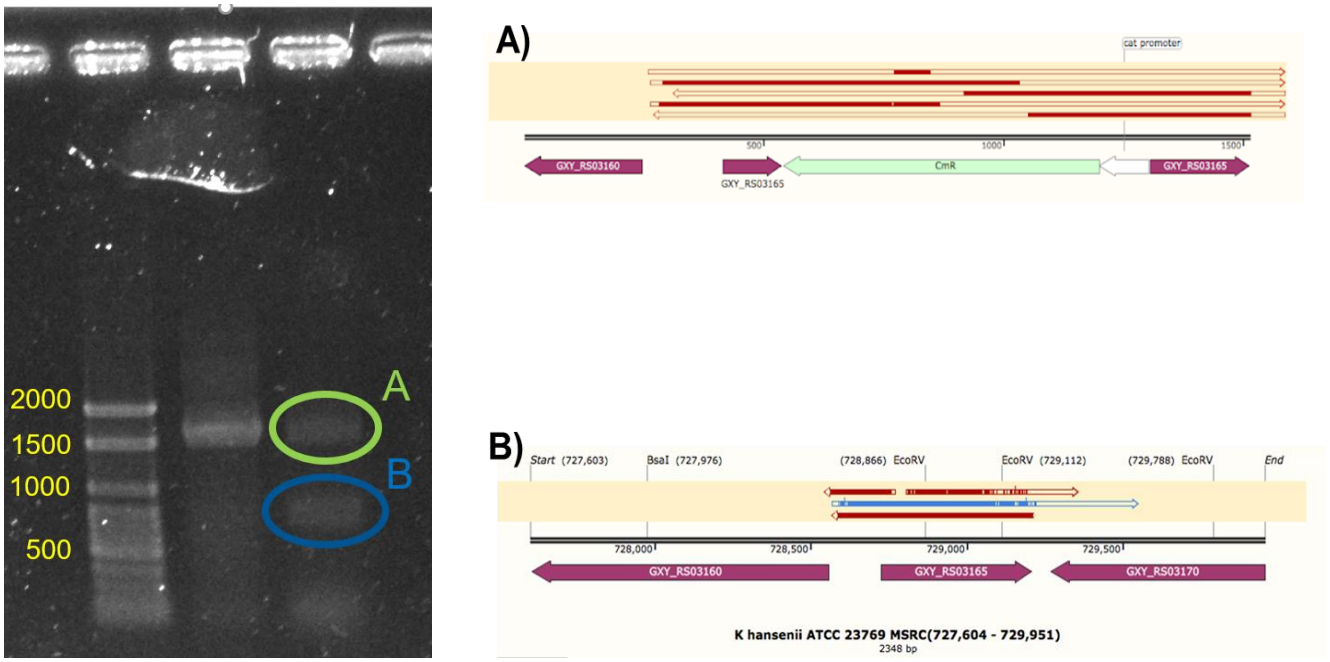

Figure 11. Confirmation of the complementation construct by agarose gel electrophoresis of PCR-amplified *msrC* using pUCD2::*msrC* extracted from the Δ*msrC* complement strain as template (agarose gel, left) Lane 1 is Ultraranger ladder by Norgen, Lanes 2 & 3 are separate PCR amplification attempts of plasmid extractions from the complement. The gel was 1% agarose in TAE buffer, stained for 10 minutes in 10 µg/mL ethidium bromide. The ~1500 bp amplified product is highlighted in green and the ~700 bp amplicon is highlighted in blue. Alignment of the sequence obtained from the green-highlighted band to the *CmR* antibiotic cassette within the Δ*msrC* mutant (A). Alignment

of the sequence obtained from the blue-highlighted band to the native *msrC* region found in WT *K. hansenii* (B).

3.2.1 Confirmation of pUCD2 Plasmid Transformation in Wild Type (WVC) and Mutant (MVC) Control Strains

To verify the transformation of pUCD2 into WT and *ΔmsrC* strains, plasmid DNA was extracted from the WVC, MVC and WT (as the negative control). Analysis by agarose gel electrophoresis shows a band at approximately 24 kb present in both the WVC and the MVC but not in the WT (Figure 12). This observation along with the spectinomycin and ampicillin resistance of both WVC and MVC confirm that the pUCD2 plasmid was successfully transformed.

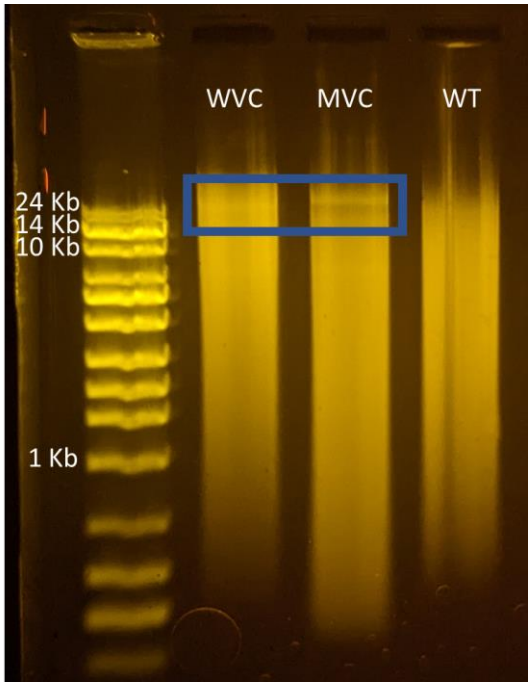

Figure 12. Gel electrophoresis of plasmids extracted from WVC (lane 2), MVC (lane 3), and WT *Komagataeibacter hansenii* (lane 4). pUCD2 plasmid is indicated by the blue rectangle. The gel was 1.0% agarose in TAE buffer, with the Norgen UltraRanger ladder (lane 1).

3.3 Carbon Source Affects Pellicle Yield of *Komagataeibacter hansenii* Δ*msrC*

To assess pellicle formation across the different bacterial strains studied in this thesis, an analytical balance was used to measure their mass. This involved weighing an empty microcentrifuge tube and subtracting the mass from the same tube that contained pellicle. However, this method did not reveal any measurable difference for any of the strains with the volume of culture used in the assay (data not shown)**.**

Given the importance of cellulose as an extracellular polysaccharide in *K. hansenii*, and to determine whether carbon source and/or the Δ*msrC* mutation impacts the cellulose output in pellicles, the anthrone assay was used to quantify the glucose equivalent in each pellicle.

Challenges arose when attempting to measure pellicle production in the complemented strain. Contrary to producing a robust pellicle, the complemented strain formed a thin, fragile film at the air-liquid interface. The film lacked structural integrity where, even when removing the culture vessels from the incubator as gently as possible, the film either disintegrated at the slightest jostle or when attempting to remove them from the growth media would consistently dissociate making processing impossible. While it was a film at the air-liquid interface, due to it lacking any physical integrity, it was deemed that what was produced by the complement did not match the definition of pellicle and consequently, no further attempts were made to quantify its cellulose content.

Interestingly, the carbon source impacted cellulose content differently among the strains (Figure 13). Both the Δ*msrC* mutant and MVC showed significantly more ($p < 0.05$) glucose equivalence when grown in fructose compared to glucose whereas the WT and WVC did not reflect that trend; the WT showed no significant change ($p < 0.05$) in

glucose equivalence with respect to the carbon source. Conversely, the WVC produced 56 mg more glucose equivalence when grown in in glucose rather than in fructose. Notably, the pellicle yield of MVC in fructose increased by 85 mg of glucose equivalence. The Δ*msrC* mutant produced the most cellulose among all tested strains with 515 (+/- 43) mg in glucose and 564 (+/- 32) mg in fructose.

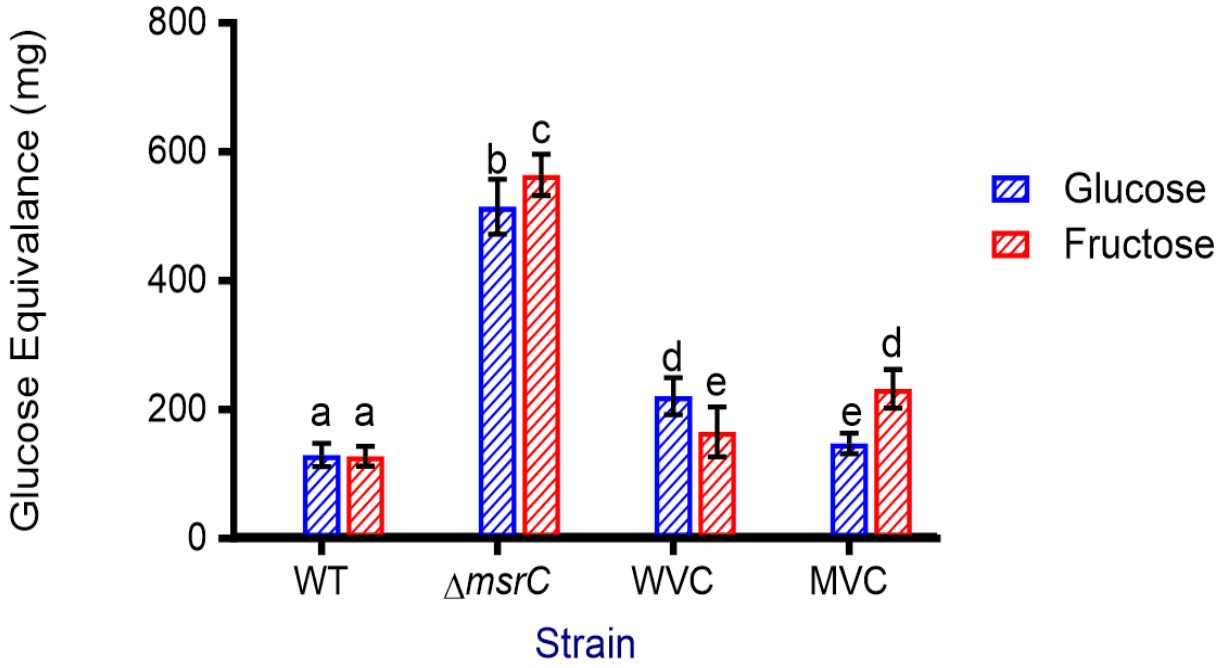

Figure 13. Cellulose yield of *Komagataeibacter hansenii* (WT), *K. hansenii ΔmsrC* (ΔmsrC), *K. hansenii*//pUCD2 (WVC), and *K. hansenii ΔmsrC*//pUCD2 (MVC). Cellulose yield measured in glucose equivalence in mg as determined by anthrone quantification. Cellulose pellicles were examined in glucose and fructose carbon source containing media. It should be noted that the complement did not produce any pellicle and therefore data is not shown. All experiments were performed in triplicate with three biological replicates and three technical replicates (n=9). Data was analyzed using a two-way ANOVA. Data was considered significant if statistically significant if $p \leq 0.05$. Distinct letters (a-e) indicate statistically different values.

3.4 MsrC Affects the pH Tolerance of *Komagataeibacter hansenii* in Stationary Cultures

As a preliminary means to determine whether pH had any effect on the growth kinetics of the *K. hansenii* strains (WT, Δ*msrC*, WVC, MVC and complement), the impact of SHG media adjusted to pH: 4, 4.5, 5, 5.5, 6, 6.5, and 7 on growth were compared to growth in unaltered SHG in a stationary growth environment. It should be noted that the pH of SHG without any pH adjustment is 5.2). The aim of this experiment was to observe the growth patterns across the pH spectrum and to identify notable

deviations compared to growth in pH 5.2 which would merit further investigation as described in 2.6.

At the conclusion of the 96-hour observation period, WT *K. hansenii* showed enhanced growth at pH 4 (Figure 14 A). No other notable differences were observed across all tested conditions for the WT. The Δ*msrC* mutant showed sensitivity to pH 6.5 with greater impedance of growth observed at pH 7 (Figure 14B). The WVC exhibited an extended lag phase in all tested conditions, only beginning to transition into the exponential growth phase towards the end of the observation period (Figure 14 C). The MVC showed a decrease in growth at pH 7, while growth at the other tested pH levels was relatively similar to the growth of the Δ*msrC* mutant (Figure 14 D). The complement strain (pUCD2::*msrC*), also showed a sensitivity to pH 7, and overall, grew more slowly reaching an OD_{600} of about 1.5 (Figure 14 E) which is comparable to that of WT but unlike the Δ*msrC* mutant and MVC, which for most pHs tested, reached OD_{600} 1.5 - 2.0. The consistent growth reduction at pH 7 observed for the Δ*msrC*, MVC, and complement strains was an interesting trend that warranted more thorough investigation through the growth kinetics experiment detailed in section 2.6.

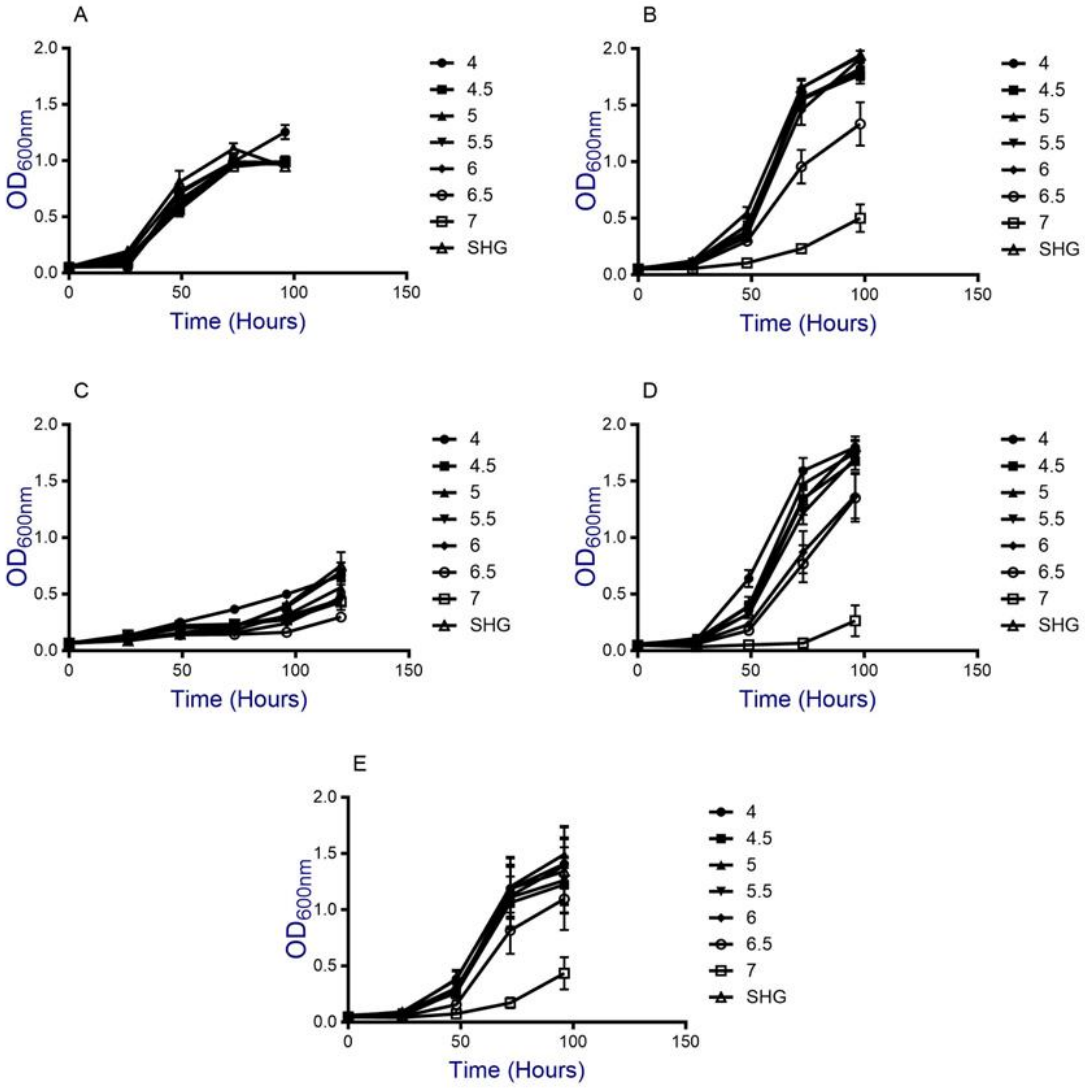

Figure 14. Stationary pH tolerance of WT (A), Δ*msrC* (B) , WVC (C), MVC (D) and complement (E). The pHs tested were 4, 4.5, 5, 5.5, 6, 6.5, and 7. Condition of growth measured in OD_{600} with measurements taken every 24 hours for 96 – 120 hours. All experiments were performed in triplicate (three biological replicates and three technical replicates) n=9.

3.4.1 Comparison of Stationary pH Tolerance Between Different WVC Transformants

To determine whether the differences in growth observed for the WVC compared to the other strains (WT, Δ*msrC,* MVC, and complement) reported in section 3.4 were due to the pUCD2 plasmid or due to effects related to transformation, two additional transformants derived from the same electroporation event as the WVC (referred to here as "Original") were tested. Their growth was monitored in standard SHG media and in SHG at pH 7. These two conditions were selected based on the results obtained in section 3.4; pH 7 was found to have a significant decrease in the growth of WVC and growth in SHG (pH 5.2) served as another point of comparison as the baseline.

The growth patterns of the two new transformants in SHG more closely resembled each other and differed from the "Original" WVC strain, which exhibited a long lag phase in SHG that was not observed with the two additional transformants (Figure 15). After the initial 24 hours of growth, the additional transformants entered exponential growth phase more similar to the results observed for the WT as reported in section in 3.4 (Figure 14), even ending the observation period at OD_{600} ~ 1.3 which also bears more resemblance to the OD_{600} of WT as reported in section 3.4 (Figure 14).

Interestingly at pH 7, the "Original" WVC strain and the two additional transformants behaved similarly with a long lag phase. By the 96-hour time point, all three transformants stayed below OD_{600} 0.5 (Figure 15), indicating a similar response to elevated pH.

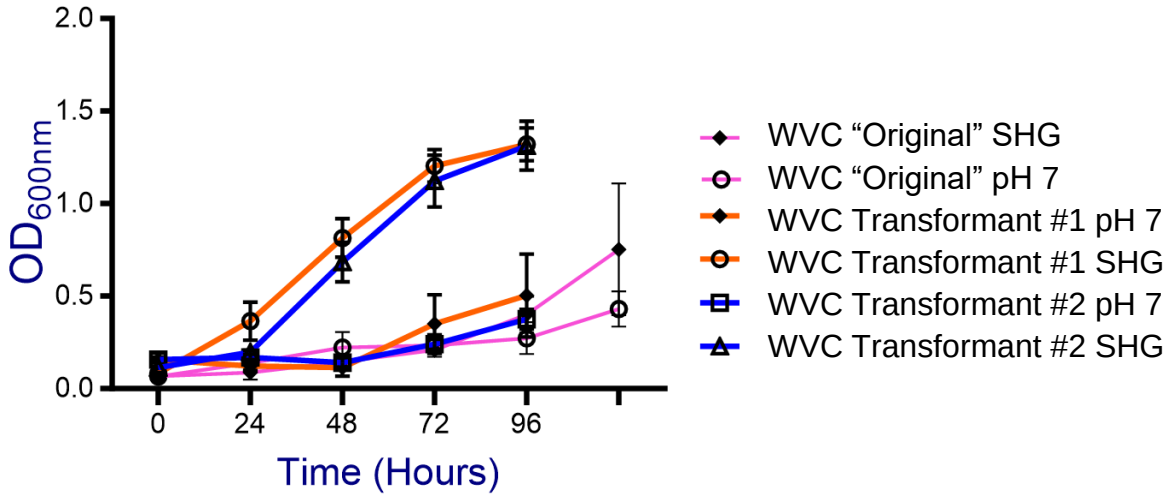

Figure 15. Growth comparison of two additional WVC transformants with the "Original" WVC transformant used for this thesis. The two additional transformants derived from the same electroporation event are "Transformant #1" and "Transformant #2". Comparisons of all transformants were made between SHG at unaltered pH (5.2) and SHG pH 7. Growth of transformants was assessed by measuring OD_{600}. All experiments were performed in triplicate with three biological replicates and three technical replicates (n=9).

3.4.2 Acute Exposure to Non-Standard pH Does Not Affect *Komagataeibacter hansenii* Viability

To determine the survivability of *K. hansenii* strains after acute exposure to non-standard pHs, the five strains (WT, Δ*msrC*, WVC, MVC, and complement) were standardized to OD_{600} of 0.5, exposed to the pHs 4, 6, and 7 for one hour. After exposure, the strains were 10-fold serially diluted and spot-plated on SHG agar plates. The control was exposure to SHG (~ pH 5.2). The CFUs of each spot with countable colonies were counted and divided by the CFUs obtained for the SHG control and multiplied by 100 to obtain % survival.

There was no significant ($p < 0.05$) change in the % survival of any of the tested strains in any of the tested pHs over the 1 hour exposure period (Figure 16).

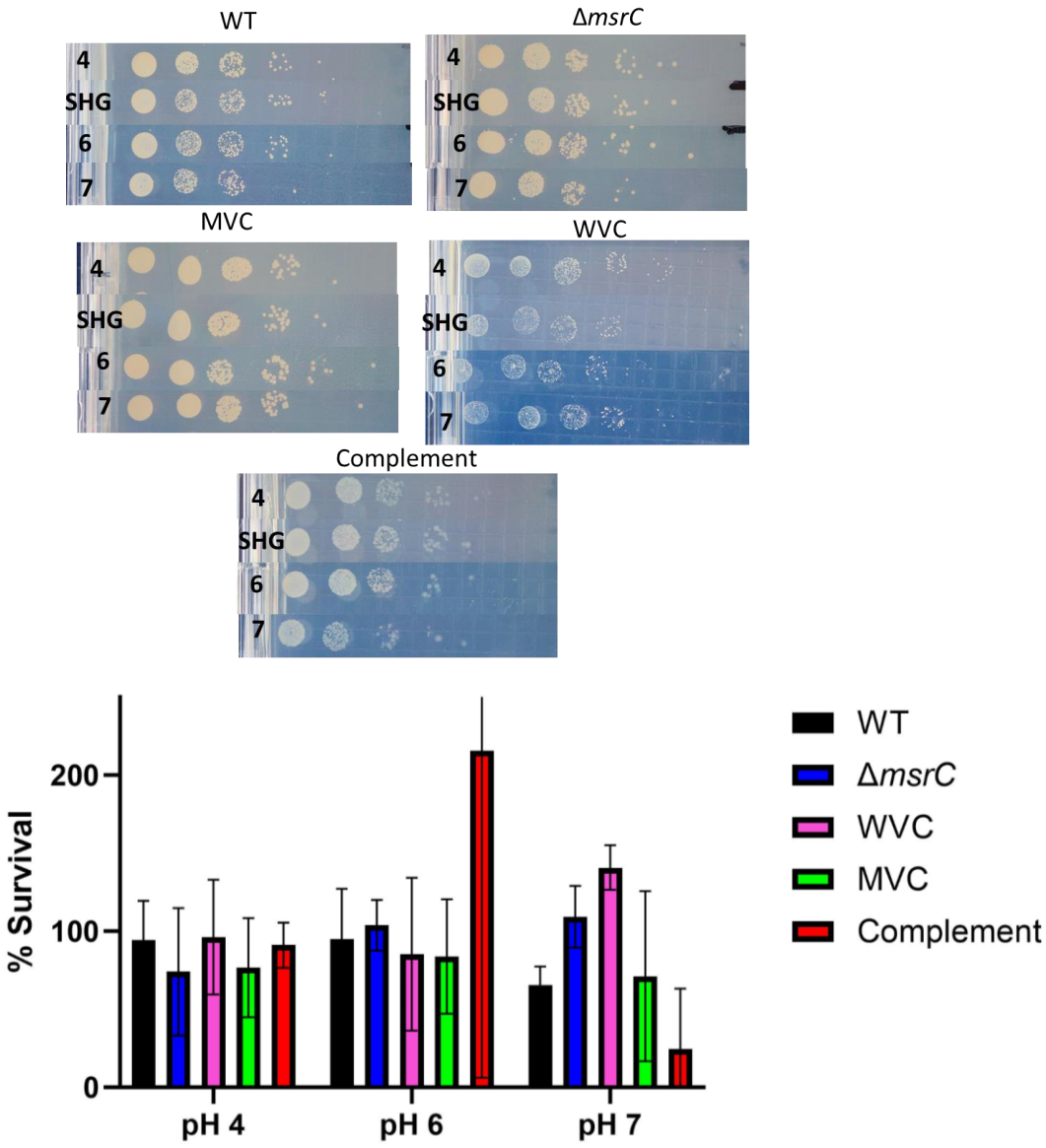

Figure 16. Survivability of *K. hansenii* strains (WT, Δ*msrC*, WVC, MVC and complement) determined by CFU for SHG at pH 4, 6 and 7 and unaltered SHG (pH 5.2). Ten-fold serial dilutions were spot-plated on SHG agar plates starting at 10^0 at the left side of the plate, decreasing by 10^{-1} concentration per spot to the right (Top). The % survivability was determined by dividing the CFUs of pH 4, 6, and 7 by that of SHG and multiplied by 100. Percent survival was plotted on a bar graph (bottom). All experiments were performed in triplicate with three biological replicates and one technical replicate (n = 3). No presence of lettering above bars indicates that there was no statistically significant ($p<0.05$) change in reported means, statistical analyses was done using a two-way ANOVA.

3.5 MsrC Controls the Growth Kinetics of *Komagataeibacter hansenii*

To determine if the Δ*msrC* mutation, pUCD2 plasmid, or the pUCD2::*msrC* complementation construct had any effect on the rate of growth of *K. hansenii*, a growth kinetics experiment was conducted to look at the effects of phytohormones (10 μM IAA, 10 μm ABA, and 1 mM ethylene), 10 μM hydrogen peroxide, and a range of environmental pHs: 4, 5, 6, and 7 to further investigate the pH effect (Figure 17).

The WT strain showed a robust growth pattern between tested conditions that rarely varied except notably in the presence of 10 μM ABA (Figure 17 C). The common trend in all conditions for WT (Figure 17), with the exception of ABA, was an early exponential growth phase within approximately 25 hours that transitions to a stationary phase at around OD_{600} 0.5-0.75 at 50 hours. In ABA (Figure 17), the WT adopted a growth pattern that mirrors the WVC with an early entry into stationary phase at an OD_{600} of 0.25 at approximately the 25-hour mark.

Both the Δ*msrC* mutant and MVC consistently outpaced the growth of the WT in all experimental conditions while behaving similarly to each other in all conditions with the exception of ABA. In 10 μM ABA supplemented cultures, the Δ*msrC* mutant, MVC, and complement behaved similarly between each other with the Δ*msrC* mutant growing the least well between the three. Interestingly, the only observed instance of the complement surpassing the growth of the Δ*msrC* mutant was in the 10 μM ABA supplemented cultures (Figure 17 C).

The Δ*msrC* mutant exhibited better growth in the same time-frame compared to the WT in every condition tested (Figure 17). However, three conditions had noticeable impacts on the growth of the Δ*msrC* mutant compared its growth pattern in SHG, these were the 10 μM ABA (Figure 17 C), pH 6 (Figure 17 H) and pH 7 (Figure 17 I) conditions where growth was noticeably slower and where the final OD_{600} was 1.0 as opposed to an OD_{600} of 1.5 as was observed when cultures were grown in SHG.

As the pH increased from pH 5 - pH 7 (Figure 17 G - I), the complement exhibited an increasingly longer lag phase before beginning to show signs of growth with complete inhibition of growth at pH 7. This was the only instance of complete growth inhibition in any of the strains or conditions tested.

Similar to the results obtained in section 3.4, the WVC had a consistent growth profile that remained consistent in all tested conditions except for pH 7 (Figure 17 I). When grown in SHG at pH 7, the WVC showed growth patterns that more closely resembled Δ*msrC* mutant and MVC with a longer lag phase and with increased overall growth compared to the growth of WVC in SHG.

An examination of the doubling time for all the strains tested (WT, Δ*msrC*, WVC, MVC, and complement) under each condition (SHG, IAA, ABA, Ethylene, H_2O_2, pH 4, 5, 6, and 7), revealed that the complement strain showed the greatest variability across all the tested conditions (Figure 18). In every testing condition that the complement was able to grow in (except pH 7) the complement showed a longer doubling time than all other strains (Figure 18 A-H). Despite the Δ*msrC* mutant and MVC ending the 168 hour observation period with a greater OD_{600} compared to the WT in SHG (Figure 17 A), the

WT had a shorter doubling time (Figure 18 A). This suggests that the WT has the capability to outpace the Δ*msrC* and MVC in terms of growth but it is able to self regulate growth, leading it to enter the stationary phase at an earlier time point with lower OD_{600}.

Comparing the doubling times of WT, Δ*msrC*, and complement in SHG to 1 mM ethylene, interesting changes occurred where the doubling time and its variability of the complement increased with ethylene when compared to SHG. The other strains (WT, Δ*msrC*, WVC, and MVC) did not show a similar change (Figure 18 A & D).

The only other notable change was a sharp increase in doubling time for the WVC at pH 7 (Figure 18 I). At pH 7, the only instance of WVC deviating from its consistent growth pattern was observed, and it behaved more similarly to the Δ*msrC* mutant (Figure 17 I).

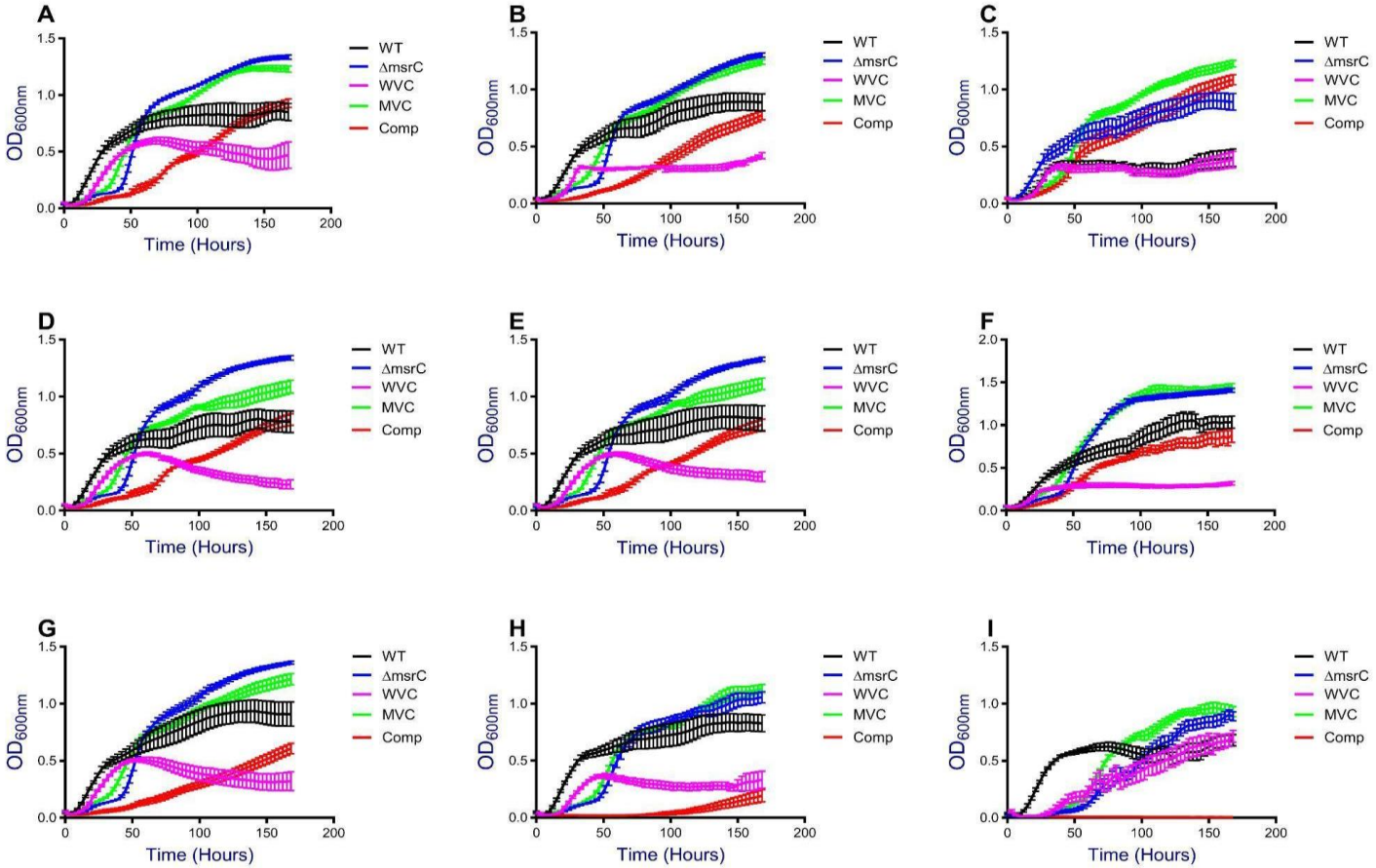

Figure 17. Growth profiles of five *K. hansenii* strains (WT, ΔmsrC, WVC, MVC and complement in various conditions. Growth measured by OD_{600}. Conditions tested included SHG (A), 10 µM IAA (B), 10 µM ABA (C), 1 mM ethylene (D), 10 µM H_2O_2 (E), pH 4 (F), pH 5 (G), pH 6 (H), and pH 7 (I). All experiments were performed in triplicate, with three biological replicates and three technical replicates (n=9).

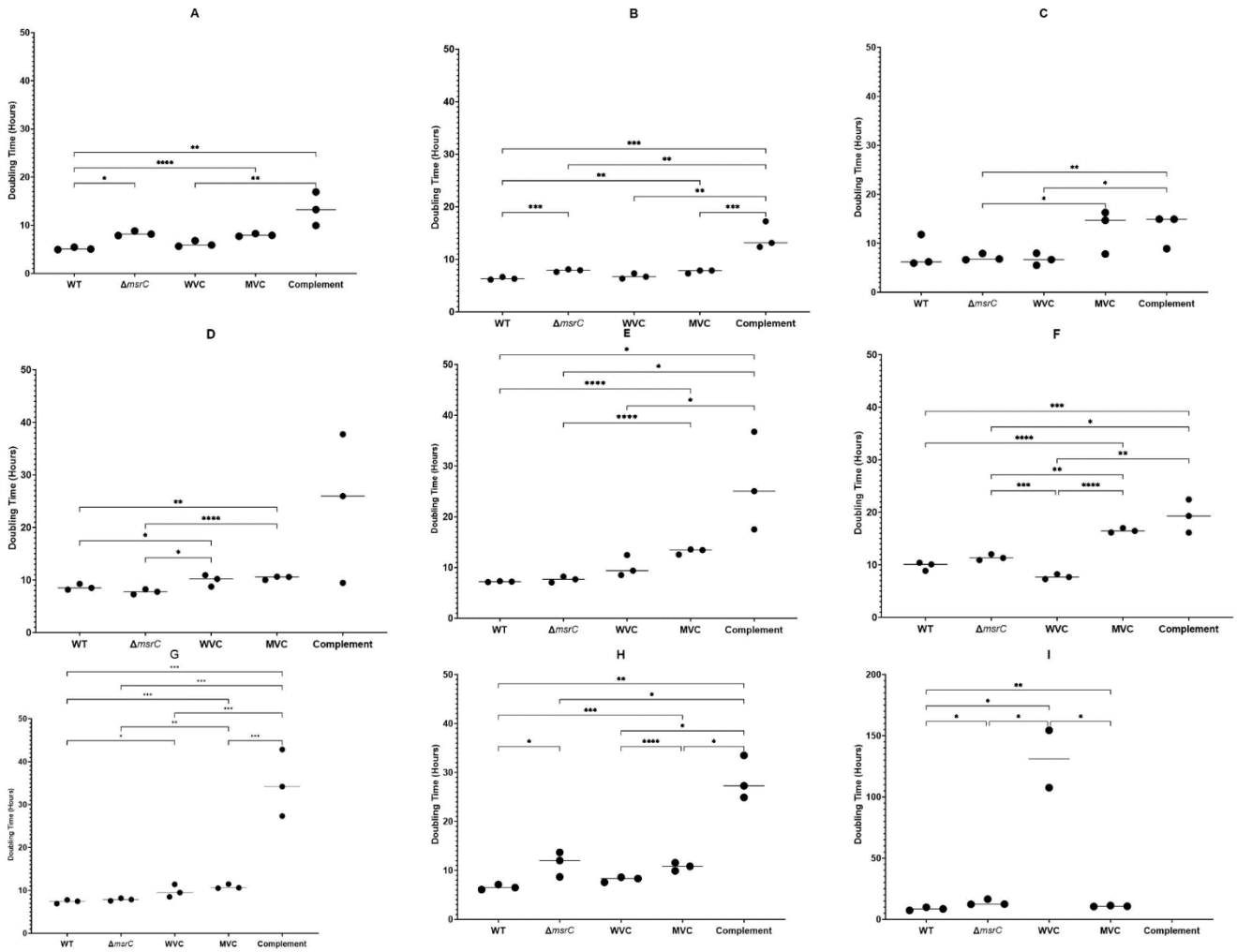

Figure 18. Doubling times of *K. hansenii* strains (WT, WT, Δ*msrC*, WVC, MVC and complement) calculated from the growth experiments shown in Figure 17. The dots represent the mean for each of three biological replicates with the horizontal bars representing the mean across the biological replicates. Conditions tested included SHG (A), 10 μM IAA (B), 10 μM ABA (C), 1 mM ethylene (D), 10 μM H_2O_2 (E), pH 4 (F), pH 5 (G), pH 6 (H), and pH 7 (I). Statistically significant data is shown in brackets labelled with asterisks to show different p values. * = $p \leq 0.05$, ** = $p \leq 0.005$, *** = $p \leq 0.0005$, **** = $p < 0.0001$. Data was analyzed using a two-way ANOVA.

3.5.1. MsrC Plays a Role in Cell Length Control in *K. hansenii* Strains

To assess the impact of IAA, ABA, ethylene, and hydrogen peroxide on the cell length of the *K. hansenii* strains (WT, Δ*msrC,* WVC, MVC, and complement), samples of the cultures grown and observed for the experiment described in section 2.6 were examined at 1000X using dark field microscopy. Cell lengths were measured from representative photos using ImageJ to calculate the Feret diameter in μm.

In SHG, the average Feret diameter of the WT was 3.2 (± 2.4) μm. Neither the WVC nor the complement strain were significantly ($p < 0.05$) different with respect to cell size (Figure 19 A). In contrast, the Δ*msrC* showed a significant ($p < 0.05$) decrease in cell size, with a mean Feret diameter of 2.0 (± 1.1) μm in SHG, remaining significantly ($p < 0.05$) shorter than the WT in all analyzed conditions.

With the exception of SHG, the cell size of MVC was not significantly ($p < 0.05$) different from the Δ*msrC* mutant in any tested condition (Figure 19). A notable trend observed for both the Δ*msrC* mutant and MVC was a consistently lower variability in cell size compared to the WT, WVC and complement strains, although the mean sizes did not differ statistically ($p<0.05$).

When grown in IAA (Figure 19 B), all strains showed similar cell length distributions with the exception of the WT and complement strain which were more variable.

In ABA supplemented cultures (Figure 19 C), WT and complement exhibited longer cells compared with Δ*msrC,* which again shows a more narrow and shorter distribution.

Interestingly, the WVC showed a marked increase in the average Feret diameter in the presence of 1 mM ethylene and in 10 μm H_2O_2 compared to SHG (Figure 19 D, E, A). It should be noted that cells of similar length to the WVC in ethylene and H_2O_2 were observed in most samples, but the greater variability in cell length yielded a lower average. A dramatic increase in the cell length variability was observed for the WVC strain when grown in ethylene (Figure 19 D) with some cells being much longer than in other conditions or strains. In the presence of H_2O_2 (Figure 19 E), the Δ*msrC* strain has notably shorter cells, while the WVC strain seems unaffected.

In all tested conditions, there was no significant difference ($p < 0.05$) in the cell length between the WT and complement strain (Figure 19). The complement, like the WT, exhibited greater variability in the cell length, as opposed to the more consistent measurements observed for the Δ*msrC* mutant and MVC strains.

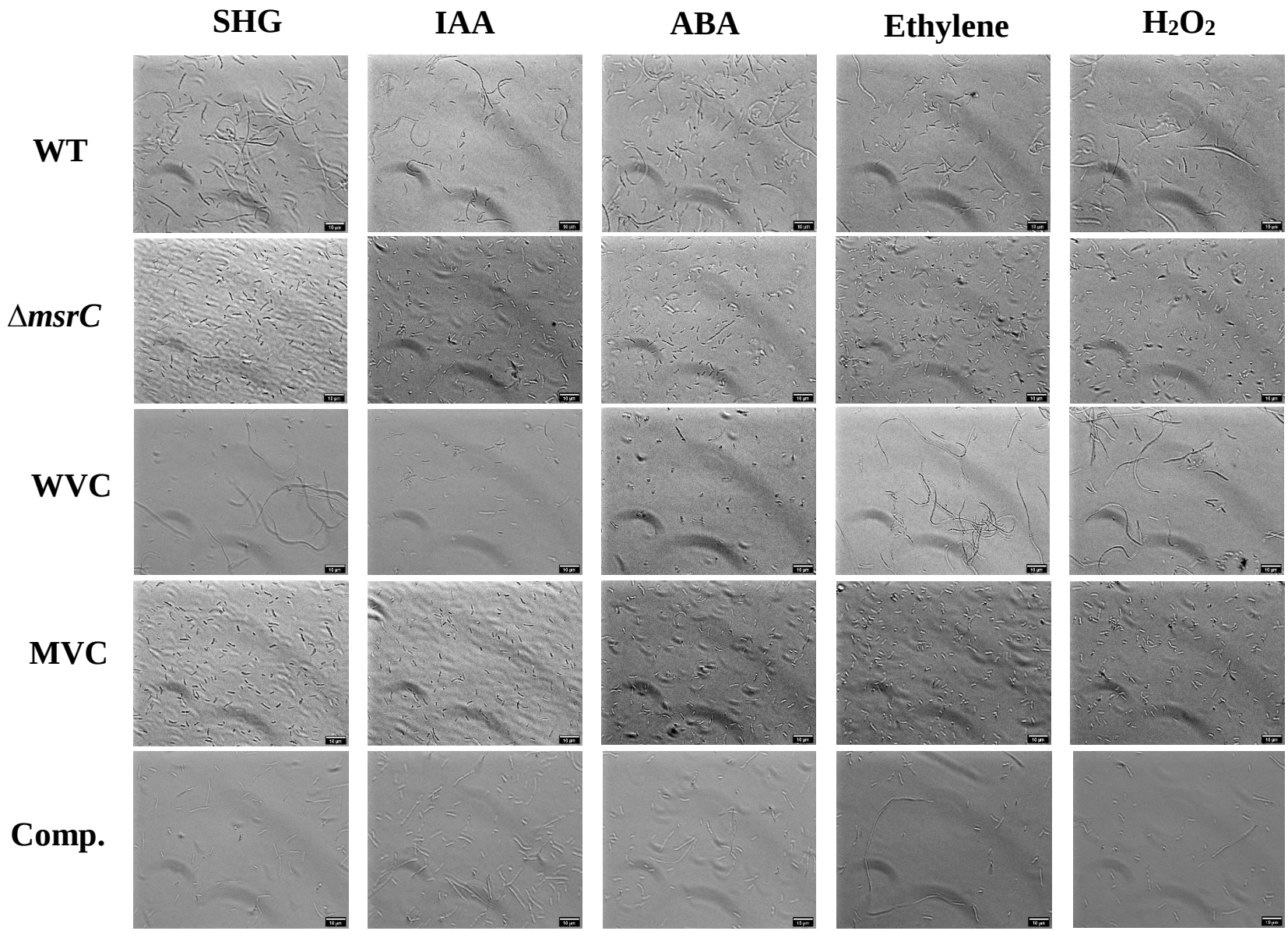
SHG
IAA
ABA
Ethylene
H2O2
WT
ΔmsrC
WVC
MVC
Comp.

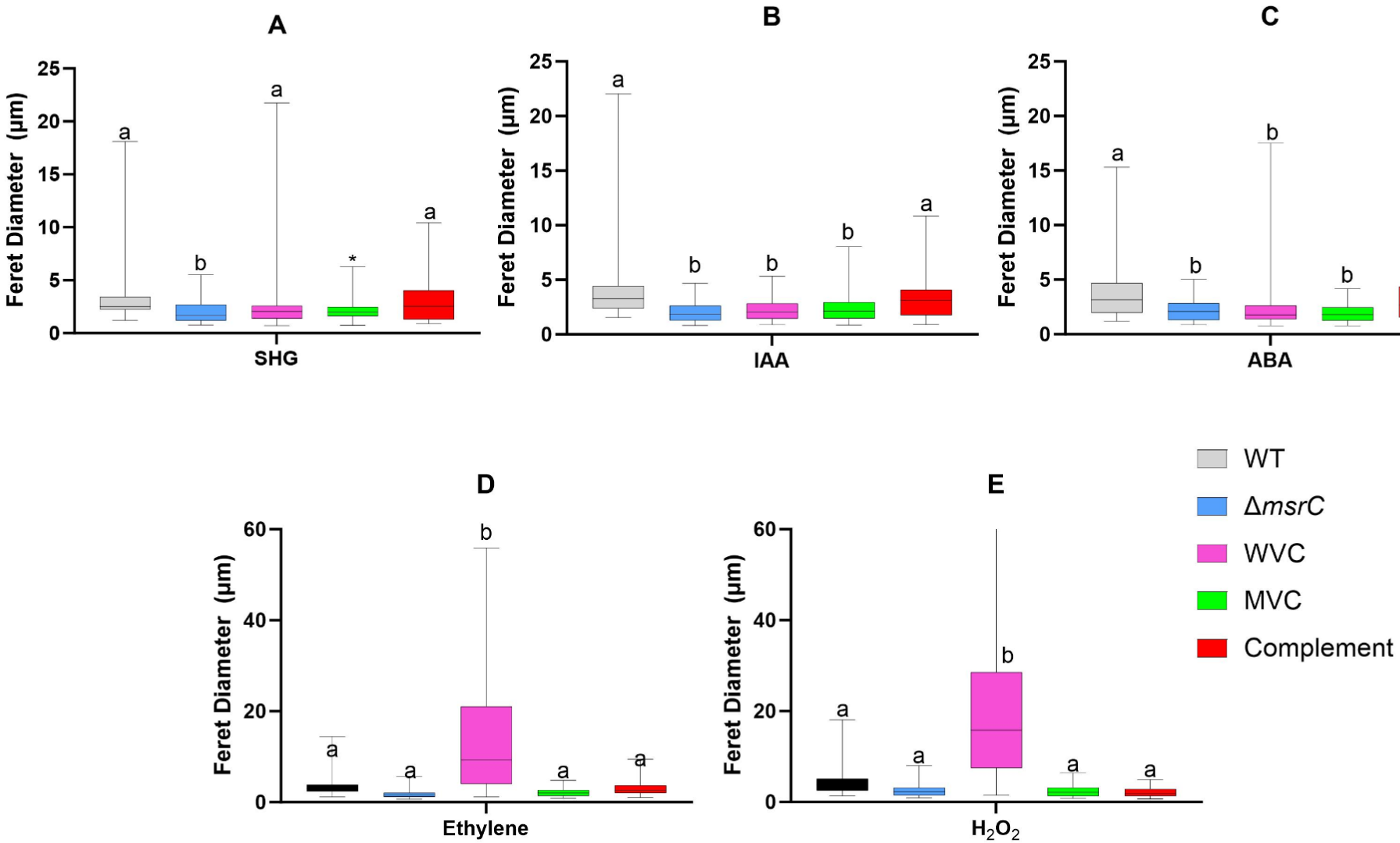

Figure 19. Cellular morphology representative photos of WT, Δ*msrC*, WVC, MVC and complement *K. hansenii* after 7 days of incubation in SHG, 10 µM IAA, 10 µM ABA, 1 mM ethylene and 10 µM hydrogen peroxide. Scale bar represents 10 µm (top). Box and whisker plot of cell diameter of WT, Δ*msrC*, WVC, MVC and Complement *K. hansenii* after 7 days of incubation exposed to SHG (A), 10 µM IAA (B), 10 µM ABA (C), 1 mM ethylene (D) and 10 µM hydrogen peroxide (E). Cell diameter determined by Feret diameter as measured by the software imageJ. Random fields of view were photographed and cells measured until an n value of approximately 60. Data was analyzed using a two-way ANOVA. (Bottom)

3.6 Comparison of Colony Morphology *Komagataeibacter hansenii* Strains

To compare morphological differences among *K. hansenii* strains (WT, Δ*msrC*, WVC, MVC, and complement), isolated colonies of each strain was streaked onto fresh SHG agar plates containing appropriate selective antibiotics. After 7 days of incubation, individual colonies of the strains were photographed to document their appearance.

A consistent colonial phenotype was observed for the WT, Δ*msrC*, WVC and MVC (Figure 20). This phenotype was characterized by raised vertical growth in a dome-like shape. This was accompanied by high structural integrity where if any colonies of these four strains were picked for inoculation with an inoculating loop, the entire colony would hold together during transfer.

In contrast, colonies of the complement strain had a flat elevation, lacking the dome-like structural elevation or structural integrity observed for the other strains (Figure 20); colonies of the complement strain look significantly different from the WT and Δ*msrC*. The complement would spread out wider than any of the other strains, remaining constrained to the surface of the agar and possessed a semi-mucoid integrity where when picking up colonies of the complement with an inoculating loop, it took less effort for the colony to come apart, indicating a less integrated colony structure. Colonies of the complement also exhibit a scalloped margin. These observations show that the process of complementing the deleted *msrC* gene does not fully restore the colonial phenotype.

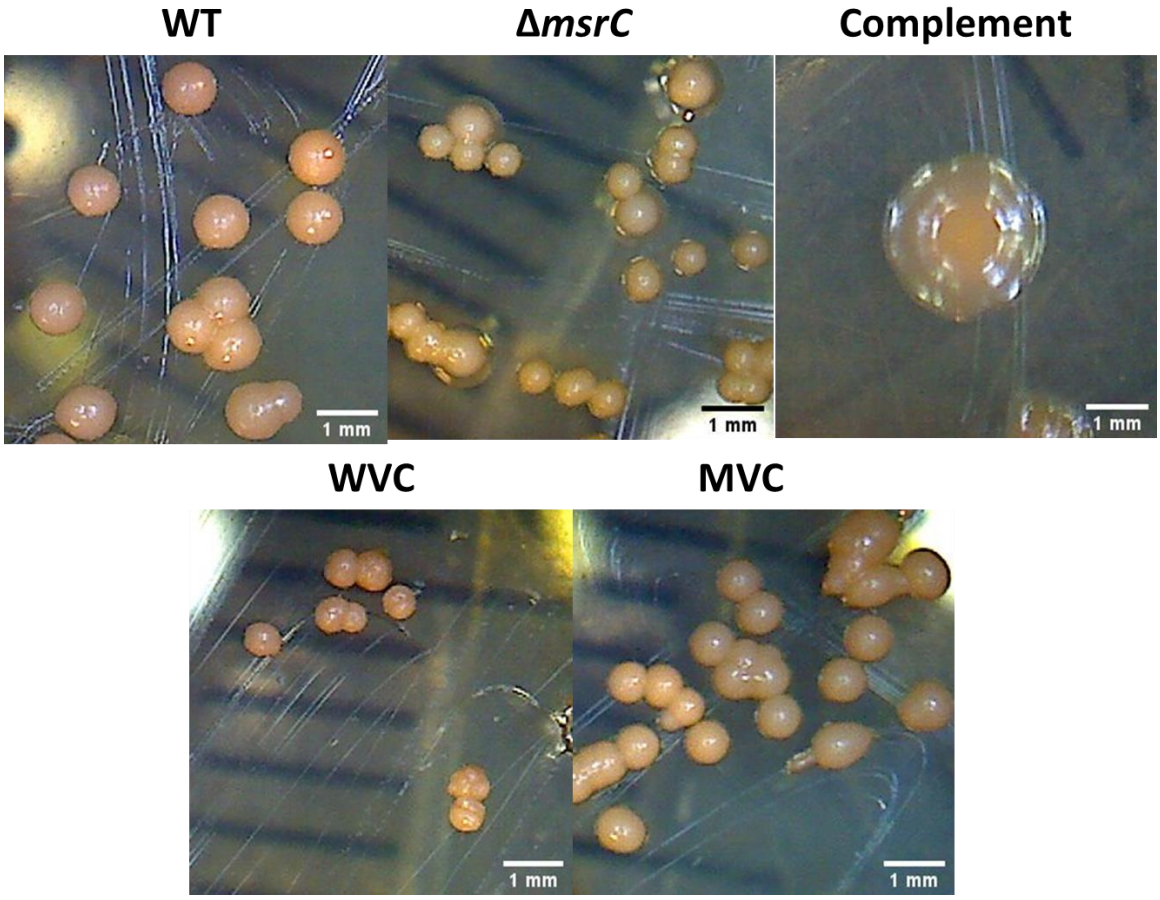

Figure 20. Colonial morphology of *K. hansenii* strains (WT, ΔmsrC, WVC, MVC, and complement). Scale bar represents 1mm. Each photo is a representative of the entire population as observed on the agar plate.

3.7 Reactive Oxygen Species Content Quantified by DCF

To investigate the ROS defence system of *K. hansenii*, cultures of each of the five strains (WT, Δ*msrC*, WVC, MVC, and complement) were exposed to oxidative stress in the form of 1 mM hydrogen peroxide. DCF staining was used to monitor their ROS processing capabilities.

Interestingly, over the 30-minute time frame, no substantive changes were observed, rather, there were only subtle and steady changes (Figure 21). As expected, cultures treated with 1 mM hydrogen peroxide exhibited higher fluorescence levels

compared to the untreated control (0 mM H_2O_2), indicating increased ROS (Figure 21). The WT exhibited the greatest change in fluorescence upon 1mM hydrogen peroxide treatment (Figure 21). In contrast, the other strains (Δ*msrC*, WVC, MVC, and complement) exhibited less dramatic fluorescence changes upon exposure to hydrogen peroxide. The untreated cultures showed a steady homeostatic level of measurable ROS, however, in the WT, ROS gradually increased over time (Figure 21A).

The Δ*msrC* mutant and MVC strains showed comparable ROS processing capabilities (Figure 21A). The WT and WVC strains differed markedly in fluorescence when exposed to 1 mM hydrogen peroxide, with WVC approaching the homeostatic levels of the WT. The response of the complement strain was more aligned with the WVC than either the Δ*msrC* mutant or the MVC strains.

Looking at the fluorescence values at the end of the 30-minute observation period, it can be seen that in all strains, the 1mM hydrogen peroxide was able to significantly ($p<0.05$) increased the fluorescence compared to homeostatic levels (Figure 21B). At homeostatic levels, WT had the most significantly ($p < 0.05$) reported ROS while the WVC exhibited the least ROS ($p < 0.05$) with the remaining three strains (Δ*msrC*, MVC, and complement) showing no significant ($p<0.05$) changes in their homeostatic ROS levels.

Similar to the untreated control, the WT had the greatest amount of fluorescence. The Δ*msrC* mutant and the MVC showed no significant ($p<0.05$) difference between their reported fluorescence. Similarly, the WVC and complement strains showed no

significant ($p < 0.05$) difference in fluorescence. However, the WVC and complement exhibited significantly ($p < 0.05$) more fluorescence than the Δ*msrC* mutant and MVC.

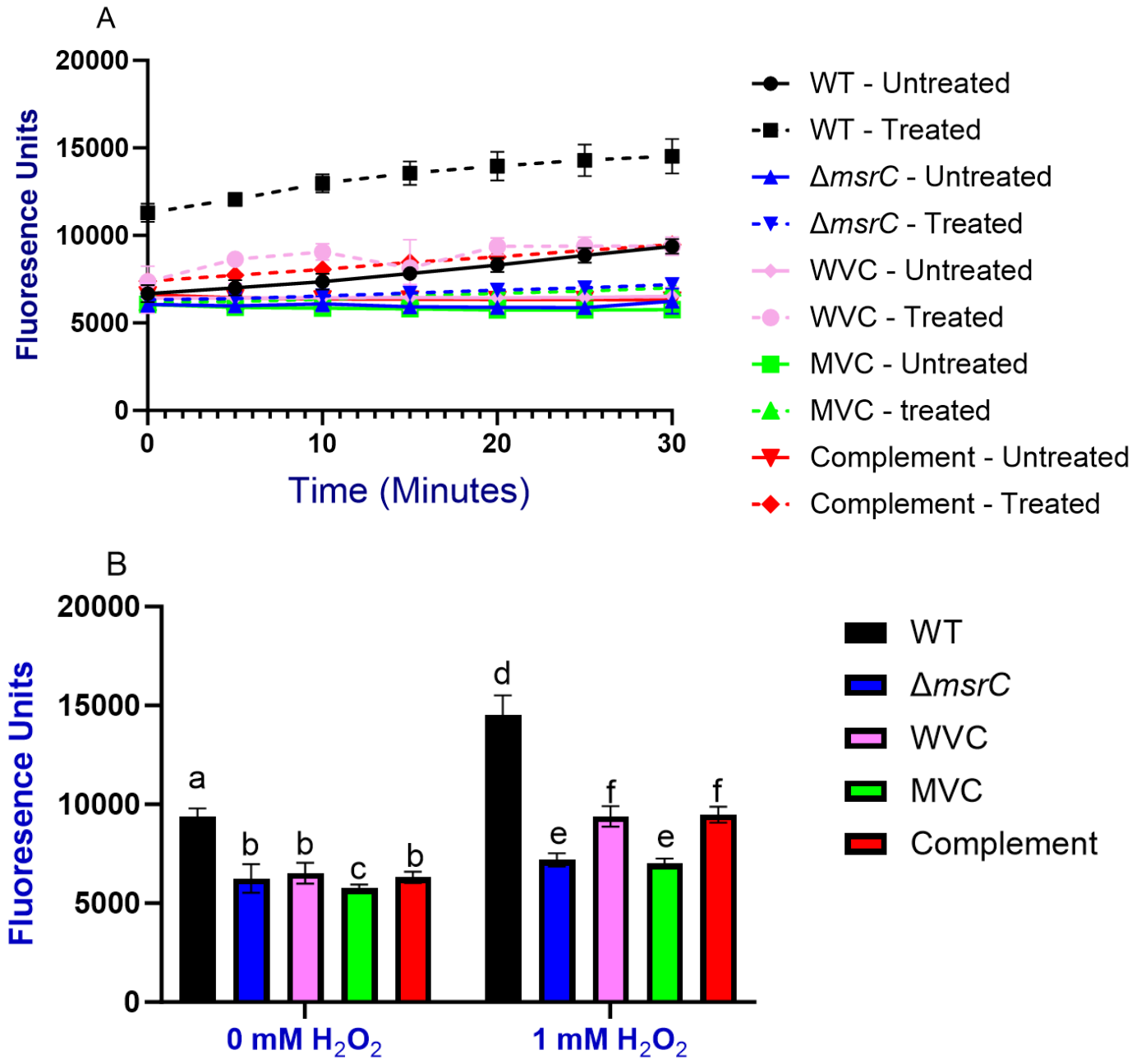

Figure 21. Intracellular reactive oxygen species (ROS) in *K. hansenii* strains (WT, Δ*msrC*, WVC, MVC, and complement) quantified by measuring DCF fluorescence. Observations were conducted over 30 minutes and the levels of ROS were measured at 5 minute intervals after exposing the strains to 1 mM H_2O_2 or the control (0 mM H_2O_2) (A). Comparison of the fluorescence of strains at the end of the 30 minute observation period between 1mM and 0 mM H_2O_2. All experiments were performed in triplicate (three biological replicates and three technical replicates) n=9. Data was considered significant if statistically significant if $p \leq 0.05$. Distinct letters (a-f) indicate statistically different values. Data was analyzed using a two-way ANOVA

3.7.1 Survivability of *Komagataeibacter hansenii* Strains in Increasing Concentrations of Exogenous Hydrogen Peroxide

To evaluate the resistance of *K. hansenii* strains to oxidative stress induced by exogenous ROS in the form of H_2O_2, the five strains (WT, Δ*msrC*, WVC, MVC, and complement) were subjected to increasing concentrations of H_2O_2 over a 30-minute exposure period.

At 1 mM H_2O_2, it was found that there was no significant ($p < 0.05$) change in the % survival of any of the strains tested (Figure 22). The Δ*msrC* mutant, MVC and complement strains had no observable CFUs in the 3 mM or 5 mM treatments. The WT and WVC were able to withstand the 3 mM, but had survival rates at less than 1%. In the 5 mM treatment, while not being statistically ($p > 0.05$) significant, the WT and WVC were the only tested strains that were able to survive and visibly appeared to improve compared to the survivability in 3 mM H_2O_2.

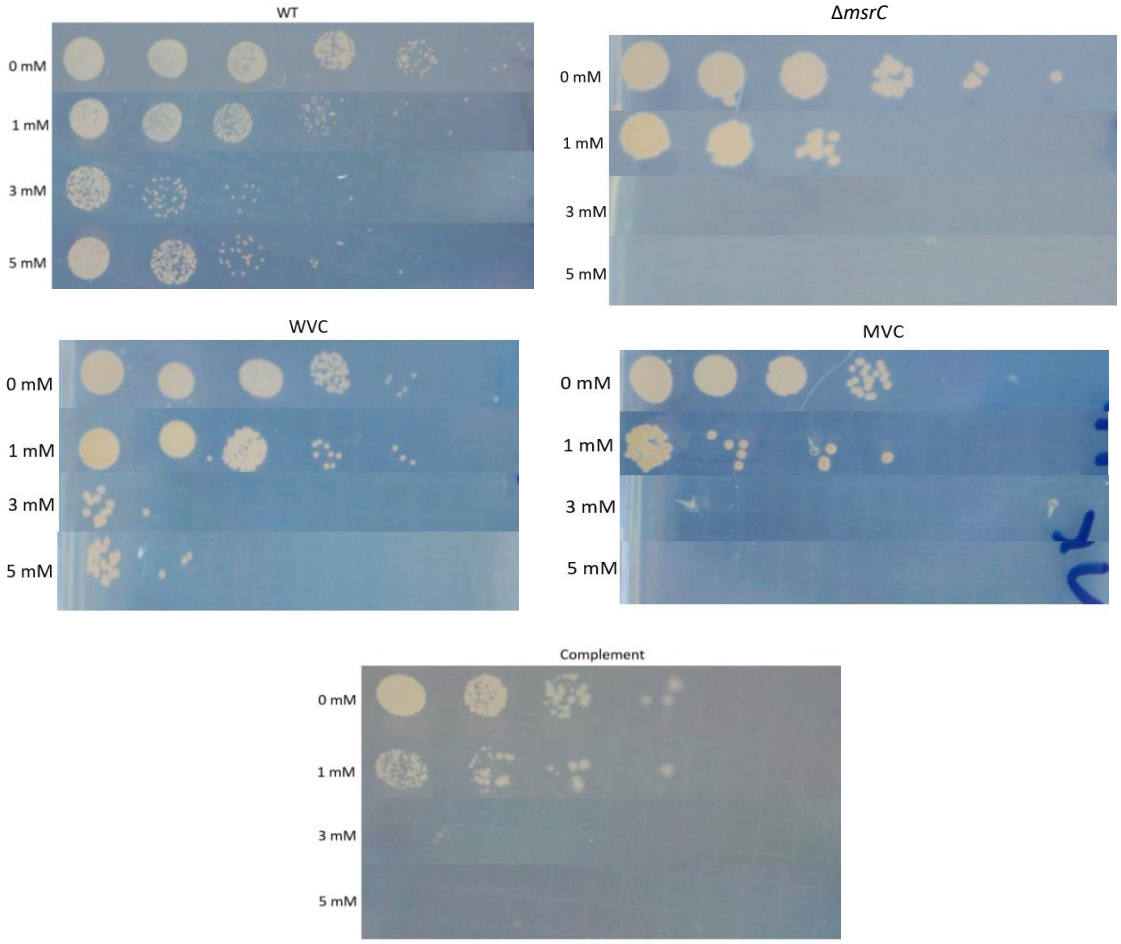
WT
0 mM
1 mM
3 mM
5 mM
ΔmsrC
0 mM
1 mM
3 mM
5 mM
WVC
0 mM
1 mM
3 mM
5 mM
MVC
0 mM
1 mM
3 mM
5 mM
Complement
0 mM
1 mM
3 mM
5 mM

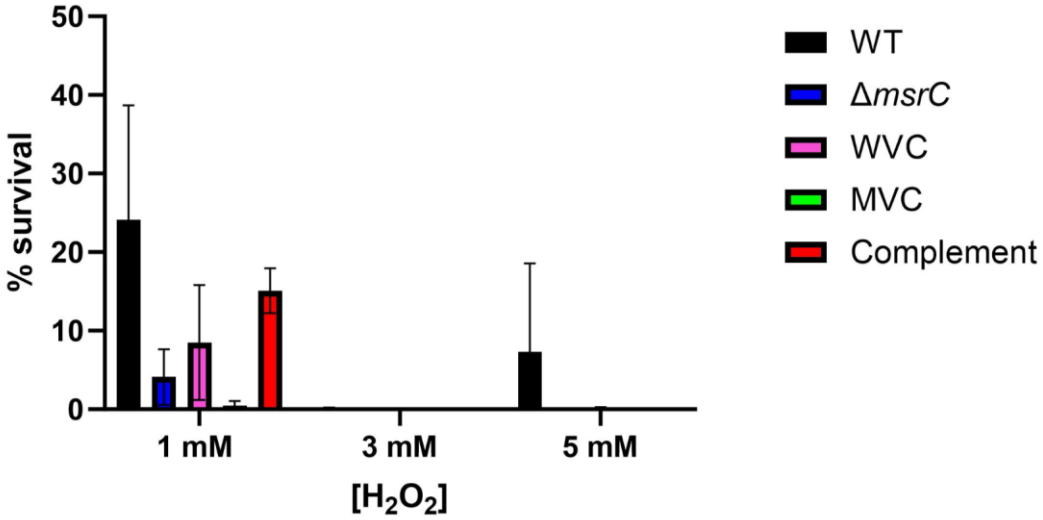
% survival
50
40
30
20
10
0
1 mM
3 mM
5 mM
[H2O2]
WT
ΔmsrC
WVC
MVC
Complement

Figure 22. Relative survival of *K. hansenii* strains (WT, Δ*msrC*, WVC, MVC and complement) at H_2O_2 concentrations of 1 mM, 3 mM, and 5 mM compared to 0 mM (untreated). Representative photos of the spot-plated 10-fold serial dilutions of cultures after exposure to the different concentrations are shown (top). Graphical representation of % survival of strains as compared to the 0 mM H_2O_2 control (bottom). Experiments were performed in triplicate with three biological replicates and 1 technical replicate (n=3). Absence of distinct letters indicate no statistical significance of data when $p \leq 0.05$. Data was analyzed using a two-way ANOVA

3.8 Extracellular AHL production of *K. hansenii* strains and Impact of Chloramphenicol and Spectinomycin on the Reporter Strain, *R. radiobacter*

To determine whether MsrC plays a role in the regulation of synthesis of AHLs, the five strains (WT, Δ*msrC*, WVC, MVC, and complement) were grown in SHG with their respective selective antibiotics until OD_{600} 0.4 - 0.6 (log phase). Samples of the cultures were harvested; the cells were pelleted by centrifugation and their supernatants collected. These supernatants were probed by the biosensor *Rhizobium radiobacter* for AHLs present in the supernatants as indicated by the formation of a blue product caused by the cleavage of X-gal by β-galactosidase as described in section 2.9. The induction of β-galactosidase by log-phase derived supernatants from each *K. hansenii* strain was compared to that of a positive control of *Pseudomonas aeruginosa* supernatant grown to the same OD_{600} range of 0.4 - 0.6.

The absorbance of the blue product was quantified by measuring the absorbance at both 615 nm and 660 nm as described in the literature (Paldrychová *et al.*, 2019; Prakash Singh & Greenstein, 2006). The wavelength did not affect the observed relationships between the *K. hansenii* strains (WT, Δ*msrC*, WVC, MVC, and complement) and *P. aeruginosa* (Figure 23A), therefore, individual comparisons between induction values determined for 615 nm and 660 nm will not be discussed.

The WT was found to produce the most extracellular AHLs present, showing to significant difference ($p < 0.05$) compared to the *P. aeruginosa* control, and significantly higher ($p < 0.05$) AHL production than the other strains tested (Δ*msrC*, WVC, MVC, and complement). Conversely, the lowest production of extracellular AHLs was observed in the Δ*msrC* mutant, MVC, and complement, with no significant difference ($p < 0.05$)

among them. The WVC, while producing significantly ($p < 0.05$) more AHLs than the Δ*msrC* mutant, MVC, and complement strains, still exhibited significantly ($p < 0.05$) less AHL activity than the WT strain (Figure 23A).

3.8.1 Quorum Sensing Impacted by Chloramphenicol and Spectinomycin

To determine if the results found in section 3.8 were solely due to the AHL content of the supernatants and not confounded by the presence of antibiotics necessary for selection of the Δ*msrC* mutant, WVC, MVC, and complement strains, a second experiment with *R. radiobacter* was attempted. This time, antibiotic presence was equalized across all supernatants. The concentrations of the diluted antibiotics (Cm and Sp) within supernatants of the MVC and complement were calculated. Subsequently, fresh aliquots of AB media were prepared to supplement the missing Cm or Sp in the supernatants to the exact same diluted concentration to match the other supernatants. After resuspension of the *R. radiobacter* in the Cm and / or Sp-dosed AB media, the antibiotic concentration was equal across all *K. hansenii* supernatant and *R. radiobacter* combinations. The resulting data was compared to supernatants of *P. aeruginosa* without the compensatory antibiotics as a positive control as well as with antibiotic compensation as another point of comparison.

Given that the *P. aeruginosa* supernatant that was used in section 3.8 was not significantly ($p < 0.05$) different compared to the WT supernatant, it acted as a WT surrogate in terms of comparison as a representative of the WT in 3.8. After antibiotic compensation, all of the reported LacZ induction values across all five strains (WT, Δ*msrC*, WVC, MVC, and complement) were not significantly ($p < 0.05$) different from

each other, but were significantly ($p < 0.05$) lower than the uncompensated *P. aeruginosa* supernatant (Figure 23B). In addition, when comparing the uncompensated *P. aeruginosa* with the exact same supernatant sample but with the addition of compensatory antibiotics, the LacZ induction significantly ($p < 0.05$) decreased, indicating that the presence of the Cm and Sp were impacting the biosensing capabilities of the *R. radiobacter*, probably through inhibiting its growth (Figure 23B).

3.8.2 Determination of AHL Content of *K. hansenii* Supernatants Without Chloramphenicol and Spectinomycin Impedance

To remove the skewing effects of the antibiotics carried over from the Δ*msrC*, WVC, MVC, and complement supernatants, these cultures were grown in SHG (no antibiotics) to the same OD_{600} as described in section 3.8. The supernatants of the cultures were harvested for AHL quantification in the same manner as described in section 3.8.

Subsequently, the same cultures were streaked onto SHG agar plates containing the respective antibiotics that were originally used for selection. This was done to ensure that the chloramphenicol resistance of the Δ*msrC* mutation or the spectinomycin resistance of the pUCD2 plasmid or pUCD2::*msrC* complementation were not lost over the culturing period in the absence of antibiotic selection which might impact the concentration of AHLs in the supernatants. This precaution ensured that any variations in AHL concentration observed in the supernatants could not be attributed to the loss of antibiotic resistance. The newly prepared supernatants were tested with fresh *R. radiobacter* culture in the same manner as described in section 3.8 and importantly, using the same *P. aeruginosa* supernatant as was assayed for the experiment described in

section 3.8 and 3.8.1. This allows for comparison across separate experiments.

The AHL content of the antibiotic-free supernatant increased substantially from what was observed and reported in section 3.8. The AHL content of the Δ*msrC* mutant and MVC were not significantly ($p < 0.05$) different from the AHL content of the control *P. aeruginosa* supernatants. Since the *P. aeruginosa* AHL level was used as a proxy for the WT, it shows that the Δ*msrC* mutant and MVC were by extension not significantly ($p < 0.05$) different from the AHL production of the WT (Figure 23C). The remaining two supernatants, WVC and complement, exhibited significantly ($p < 0.05$) lower LacZ induction compared to the Δ*msrC* mutant, MVC and *P. aeruginosa*. The LacZ induction compared between the WVC and complement was also found to not be statistically ($p < 0.05$) different from each other (Figure 23C).

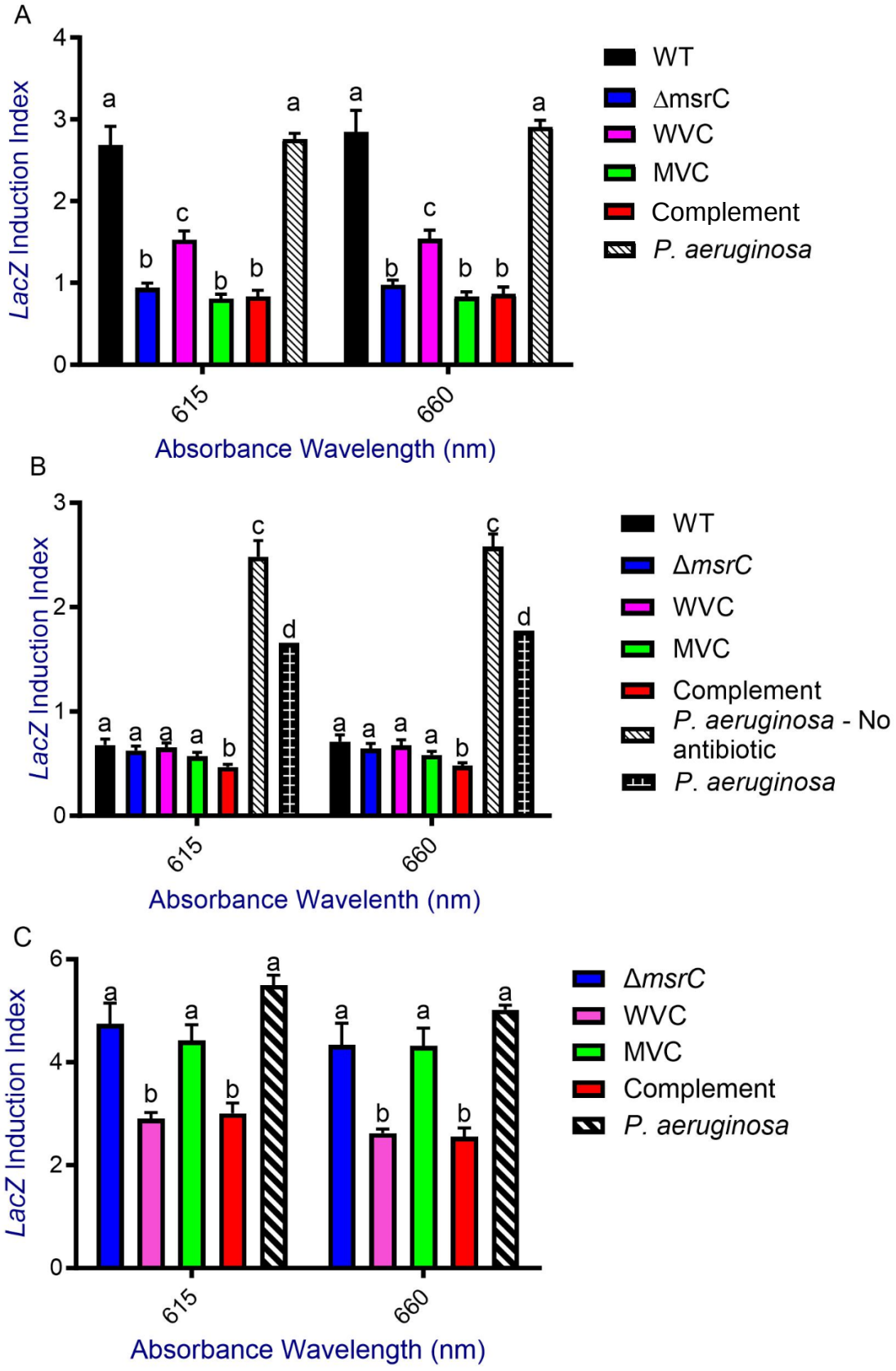
A
LacZ Induction Index
Absorbance Wavelength (nm)
615
660
WT
ΔmsrC
WVC
MVC
Complement
P. aeruginosa
B
LacZ Induction Index
Absorbance Wavelenth (nm)
615
660
WT
ΔmsrC
WVC
MVC
Complement
P. aeruginosa - No antibiotic
P. aeruginosa
C
LacZ Induction Index
Absorbance Wavelength (nm)
615
660
ΔmsrC
WVC
MVC
Complement
P. aeruginosa

Figure 23. Determination of AHL production in supernatant of *K. hansenii* strains (WT, Δ*msrC*, WVC, MVC, and complement) as detected by the biosensor *R. radiobacter*. Evaluating AHL production in supernatants with selective antibiotics (A), evaluating AHL production in supernatants with equalized antibiotic concentrations (B), and AHL production when grown in the absence of any selective antibiotics (C). Experiments were performed in triplicate (three biological replicates and 1 technical replicate) n=3. Absence of distinct letters indicate no statistical significance of data when $p \leq 0.05$. Data was analyzed using a two-way ANOVA

Chapter 4. Discussion

The goal of this thesis was to functionally characterize the GAF-domain-containing MsrC protein in *Komagataeibacter hansenii*. The thesis focussed on evaluating the consequences of deleting the *msrC* gene in *K. hansenii*, particularly looking at how it impacts the organism's response to diverse environmental stimuli. Additionally, the study included analysis of the complemented mutant as well as wild type vector control and mutant vector control with the aim of elucidating the role played by MsrC in mediating the cellular responses of *K. hansenii* to a range of external factors**.**

In this thesis, the Δ*msrC* mutant strain was successfully complemented. This was achieved by cloning the WT *msrC* gene into the shuttle vector pUCD2 and then transforming Δ*msrC* competent cells to yield *K. hansenii* pUCD2::*msrC*, referred to throughout the thesis as the complement. The wildtype vector control (WVC) and the mutant vector control (MVC) are critical components of this thesis work because they serve as a control group to help distinguish the effects caused by the deletion of the *msrC* gene and any phenotypic changes that may arise merely from the presence of the vector.

As part of the validation process for the control strains, plasmid preparations were made from cultures of WVC, MVC and WT; the latter was not expected to contain any plasmid. The plasmid extraction of the WVC and MVC showed band not present in WT (Figure 12). The presence of spectinomycin resistance along with the ~24 kb band observed in the plasmid extractions from WVC and MVC provided evidence that the pUCD2 plasmid was successfully incorporated into these strains and that it was maintained after culturing. The discrepancy between the expected 13 kb plasmid size and the observed band at ~24 kb may be due to the plasmid existing in a state that might

cause it to run higher than expected, such as if it were in the nicked open circular position, which has been shown to affect migration in an electrophoresis gel (Balagurumoorthy & Adelstein, 2008). This is plausible given that linearizing pUCD2 with *Pst*I results in a band that migrates at the expected 13 kb size.

There were notable differences observed through comparative analysis of the five *K. hansenii* strains (WT, Δ*msrC*, WVC, MVC, and complement) in regard to cellulose production (Figure 13). Since cellulose is composed of glucose monomers, we hypothesized that growing the strains in fructose-containing medium would result in a lower cellulose yield due to the additional metabolic step required to convert fructose into glucose. Contrary to our expectations, the cellulose yield observed for the WT strain was unaffected by the type of carbon source. Interestingly, carbon source did significantly impact the glucose equivalence yield for both the Δ*msrC* mutant and MVC. For these strains, cellulose yield increased when cultures were grown with fructose as carbon source compared to glucose. This observation aligns with the findings reported by Arbing (2020), where the doubling time of the Δ*msrC* mutant was lower in the presence of fructose compared to glucose. A possible explanation for the observed cellulose yield by Δ*msrC* in this thesis could be that the Δ*msrC* mutant, with its faster growth rate in fructose, outgrows the WT leading to a higher cell density, which in turn could amplify cellulose production on a per-culture basis rather than a cell-per-cell basis. One way to test this hypothesis further would be to repeat the experiment described in section 2.4 with a dual approach to assess both cellulose yield and cell density. A larger scale culture of both the Δ*msrC* mutant and MVC could be grown to stationary phase in fructose containing medium, then split into two sets of identical cultures. The one set would be

subjected to the procedure described in section 2.4.1 to confirm cellulose production and the second set would be treated with exogenous cellulase to digest the cellulosic pellicle, followed by serial dilutions as described in section 2.8.1 to quantify the number of viable cells and compared to viable counts from cultures derived from WT similarly treated. This dual assessment would help discern whether the increased cellulose yield observed for the Δ*msrC* mutant and MVC is a result of higher cell numbers or if, perhaps, these strains have an enhanced per-cell cellulose production capability when utilizing fructose as a carbon source despite the extra metabolic step required for conversion of fructose to glucose.

In the experiments conducted for this thesis, the presence of the pUCD2 plasmid coincided with a significantly reduced cellulose yield in the Δ*msrC* mutant compared to the MVC; however, this same drastic reduction was not observed between the WT and WVC (Figure 17). The reason for this could be related to the exogenous ethanol added to cultures that required chloramphenicol selection; chloramphenicol stock was prepared with ethanol. Introduction of chloramphenicol to SHG or SHF media results in 1% (v/v) ethanol. Previous work with pUCD2 in *K. hansenii* by the team of Deng *et al.* in 2015 showed that a *K. hansenii* mutant with decreased cellulose production compared to the WT was able to be complemented using pUCD2 to restore cellulose synthesis, increasing yield from 34% in the mutant to 94% in the complement compared to the WT. However, they did not report the use of vector control strains so it is uncertain whether pUCD2 would have had an impact on cellulose yield.

To address this and to investigate the impact of ethanol and chloramphenicol on cellulose yield, the experiment described in this thesis could be repeated without the

addition of the selective antibiotic. This approach would clarify their individual and combined impacts on cellulose synthesis and verify the complementation capability of the pUCD2 plasmid in the absence of these potentially confounding variables.

One of the most unexpected results obtained in this thesis work was the inability of complemented strain to produce an extracellular polysaccharide that met the definition of a pellicle. Instead of a cohesive pellicle, the complement produced what appeared to be a weakly assembled film that would readily disintegrate while attempting to conduct analyses or when transporting the culture vessel. This fragile film would start to evenly resuspend into smaller particles in the culture media, making it impossible to process in the same manner as the other strains (WT, Δ*msrC*, WVC, and MVC), which in stark contrast had robust pellicles. To overcome this challenge, the pellicle collection method could be revised from a physical removal system to a filtration-based method to better isolate the extracellular polysaccharide from the growth media. For instance, the cultures could be filtered through a glass fibre pad, separating the pellicle from the growth medium. After filtration, the glass filter and cellulose could be treated with repeated washings of NaOH and water to kill the incorporated cells and remove cellular debris so that just the cellulose (or other EPS) scaffold remains. Taking advantage of the fact that the glass filter would be unreactive with sulfuric acid in the anthrone assay, the entire filter could be immersed in the anthrone - sulfuric acid solution to determine the amount of equivalent glucose captured in the filter, allowing for the measurement of dissociated pellicle fragments, provided they are larger than the pores of the filter. This refined protocol should enable a more accurate assessment of amorphous cellulose production in cases where conventional pellicle harvesting is unfeasible.

Analysis of the growth kinetics across the five test strains revealed several interesting results that have implications for understanding the biological role of the MsrC in *K. hansenii*. During the untreated SHG growth experiment (Figure 17A), the Δ*msrC* and MVC strains initially exhibit an extended lag phase, yet once they enter exponential growth, the rate of growth is higher than that observed for the WT. Additionally, they grow to a higher density over the same time frame compared to both the WT and WVC. Interestingly, the complement grows slower than either the Δ*msrC* mutant or the MVC strains, exhibiting growth more alike to the WT and WVC, showing that the ectopic expression of *msrC* from the plasmid is directly slowing the rate of growth. Together, these observations suggest that the MsrC plays a significant role in modulating the growth kinetics of *K. hansenii.*

Another interesting observation resulting from the analysis of growth kinetics is that the Δ*msrC* mutant and MVC both exhibit biphasic growth curves as evidenced by two clear exponential growth phases with a brief lag phase in between (Figure 17). Similar growth patterns have been shown previously for *K. xylinus* which undergoes a diauxic growth pattern with a longer lag phase in the presence of 5 g/L ethanol (approximately 6% (v/v)) where the longer lag phase is due to the sequential utilization of glucose and ethanol with an intermediary lag phase corresponding to metabolic shifts (Kornmann *et al.,* 2003). The observed growth of the Δ*msrC* mutant and MVC may be explained by the strains consuming the glucose and ethanol in a similar manner since the selective antibiotic, chloramphenicol, was dissolved in ethanol and added to a 1% (v/v) concentration to SHG medium. The impact of ethanol metabolism on growth of the Δ*msrC* mutant and MVC could be determined by repeating the experiment excluding

chloramphenicol but with the addition of 1 % (v/v) ethanol to observe whether the growth changes observed in Figure 17 compared to the WT were due to the presence of ethanol or the Δ*msrC* mutation. After completing the experiment, the subsequent bacterial cultures should be streaked onto antibiotic selective media to confirm that the Δ*msrC* mutation or the pUCD2 plasmid was not lost.

The Δ*msrC*, MVC, and complement strains remained unaffected when grown in the presence of 10 µM ABA treatment, whereas the WT and WVC are clearly impacted since they show a marked reduction in growth to slightly under 0.5 OD_{600} before entering stationary phase (Figure 17C). This result shows that MsrC is involved in the cellular response to exogenous ABA, and given its GAF-domain, may have a role in ABA detection. Notably, complementation of the Δ*msrC* does not fully restore WT-like sensitivity to ABA. This finding is supported by the results of WT and WVC showing that the pUCD2 plasmid has no effect on either the detection or response to ABA, underscoring the complexity of the MsrC regulatory functions.

In contrast, when exposed to 1 mM ethylene, no discernible difference in growth was observed across all strains compared to the untreated SHG (Figure 17D). There are three possible explanations for this observation; the first being that MsrC does not play a role in ethylene detection. Second, ethylene at 1mM concentration is not sufficient to elicit a change in growth pattern, or third, that ethylene itself does not impact growth. The second and third postulation is supported by previous work in the Strap lab where in 2015, it was found that *K. xylinus* showed no alteration in growth pattern in 10 µM ethylene as compared with unsupplemented SHG (Augimeri & Strap, 2015). Considering neither *K. xylinus* nor *K. hansenii* showed any growth alteration in either 10 µM or 1 mM

ethylene, at this time it is currently inconclusive whether MsrC plays a role in ethylene perception in *K. hansenii*. However, it is noteworthy that the same paper by Strap and Augimeri in 2015 went on to report that ethylene at 10 µM did have an effect on cellulose production in *K. xylinus*, suggesting that while growth may be unaffected, other cellular processes could be responsive to the presence of ethylene. The decision to explore the effect of 1 mM ethylene with *K. hansenii* was driven by the hypothesis that higher ethylene concentrations might elicit a response not seen at lower levels, thus expanding on the scope of understanding of the impact of ethylene on *Komagataeibacter.* The absence of growth modulation at this concentration adds to the growing body of knowledge but also underscores the need for further investigation to unravel the precise role of MsrC (if any) in ethylene signaling and response.

To obtain a more definitive determination on the relationship between MsrC and ethylene detection, the five test strains could be subjected to the pellicle assay and anthrone quantification (as described in sections 2.4 and 2.4.1). This approach would consist of comparing the cellulose yield between untreated SHG and SHG supplemented with 10 µM or 1 mM ethylene as a means to determine whether MsrC plays a role in ethylene-mediated cellulose synthesis.

When looking at the effects of the Δ*msrC* mutation, the pUCD2 plasmid, or the pUCD2::*msrC* complementation construct combined with IAA, ABA, ethylene, and H_2O_2 on the physical morphology of *K. hansenii*, interesting results were observed despite the lack of statistical significance (Figure 19). The WT *K. hansenii* cultures showed a large variability in cell size, trending larger on average than the Δ*msrC* mutant and MVC. This phenotypic variability echoes the size diversity observed for acetic acid bacteria within

biofilms of fruit-based vinegars (Valera *et al.*, 2015). While the size of cells observed for the Δ*msrC* mutant were not smaller than some of the observed WT cells grown in SHG, the relative proportion of larger cells was reduced, lowering the mean cell size (Figure 19). This morphological change may be related to the enhanced growth rate observed in Figure 17A. It is possible that MsrC could play a role in cytokinesis during mitotic divisions. The Δ*msrC* mutant might have increased efficiency in cytokinesis, allowing what would have been one long cell in the WT to be four or five smaller cells in the Δ*msrC,* each working to replicate independently, leading to increased cell number and growth rate.

The most pronounced change in cell morphology was observed in the WVC cultures where exposure to ethylene and H_2O_2 led to an increase in the average cell length (Figure 19D and Figure 19E). Similar to the Δ*msrC* mutant and MVC, long cells like those observed in ethylene and H_2O_2 were present in the other conditions tested on the WVC, however, there were fewer smaller cells, which accounts for the increase in the average cell length seen on the graph. Considering the morphological variability observed for the WVC transformants (Figure 15), it is uncertain whether the drastic increase in cell size could be attributed to the pUCD2 plasmid or the transformant effects of this particular WVC representative. To resolve this uncertainty, additional WVC transformants should be examined under the same conditions to see if a repeatable increase in cell length in 1 mM ethylene or 1 μM H_2O_2 is observed.

The cell size of the complemented strain was very variable. It was more similar to the cell sizes of the WT and WVC than it was to the Δ*msrC* mutant or MVC, particularly in SHG, IAA, and ABA (Figure 19 A-C). This supports the possibility that MsrC impacts

cell size regulation. This is another phenotypic characteristic of the WT *K. hansenii* that has been restored with the *msrC* complementation.

One of the earliest observations made about the five *K. hansenii* strains (WT, Δ*msrC*, WVC, MVC, and complement) was the noticeable differences in colony size and shape. A common colonial morphology observed for the WT, Δ*msrC* mutant, WVC, and MVC was the formation of a dome-shaped colony that grew relatively high compared to the complement (convex *vs* flat). The complement showed no dome-shape in its colony nor did it raise off the agar vertically, instead it had a flat circular shape with noticeably weaker structural integrity. This colonial morphology suggests a correlation with the strain's inability to produce measurable pellicle as seen in Figure 13. This phenotype provides insights into the structural function of cellulose in colony architecture. The cellulose is likely to be providing the physical scaffolding that allows the *K. hansenii* colony to raise vertically. Being deficient in cellulose production could lead to inability of the complement to show the WT colonial morphology, leading to it appearing flat. Despite not producing cellulose for structural integrity, the colonies of the complement did have more integrity than the more butyrous colonies of *E. coli* or *P. aeruginosa*. This retained partial structural integrity of the colonies in the complement strain could be due to the complement strain leveraging other structural elements besides cellulose to help support the colony's growth such as proteins or other exopolysaccharides, albeit in lower proportions than cellulose. It is known that *K. hansenii* does produce other non-cellulosic exopolysaccharides such as galactose and mannose (Deng *et al.*, 2015) in lower proportions relative to cellulose, which could be providing weaker scaffolding compared to the cellulose-supported colonies of the WT. Altogether, the colony morphology of the

complement strain offers a visible marker of the altered cellular machinery caused by the ectopic expression of the *msrC* gene in the deletion mutant. These observations highlight the multifaceted role of cellulose not only in pellicle formation but also in maintaining the structural integrity and three-dimensional morphology of *K. hansenii* colonies. Further investigation into the quantitative and qualitative aspects of these alternative structural exopolysaccharides could shed light on their putative compensatory roles in the absence of cellulose and deepen our understanding of the structural dynamics within bacterial colonies.

In assessing the role of the MsrC in the oxidative stress response, comparisons of the impact of the Δ*msrC* mutation, the pUCD2 plasmid, and the pUCD2::*msrC* complementation construct revealed several key findings. Homeostatic levels (no additional H_2O_2) of reactive oxygen species as indicated by DCF fluorescence were highest in the WT strain compared to any other strain (Figure 21B). This paired with the observations with the 1 mM exogenous H_2O_2 where the WT strain continued to show the highest level of ROS, a pattern that is suggestive of the intrinsic oxidative stress tolerance of the WT. In contrast, both the pUCD2 plasmid and the Δ*msrC* mutation show an increased sensitivity and lethality to ROS. This view is taken because the DCF can only report on living cells, so if cells reach ROS levels that are too high to survive, they die. The cells that remain viable are able to survive at that ROS level indicated by DCF; reduced DCF-detected ROS levels. Similar results were reported by Arbing (2020) where Δ*msrC* mutant exhibited lower DCF-detected ROS without added H_2O_2 compared to the WT strain. The implication here is that the absence of MsrC may compromise cellular

defense mechanisms against oxidative damage, leading to increased cell death under oxidative stress and consequently lower DCF fluorescence.

The partial restoration of ROS tolerance in the complemented strain compared to the Δ*msrC* mutant, although not reaching the levels observed in the WT, indicates that the reintroduction of *msrC* can confer a degree of oxidative stress resilience. The complemented strain exhibited a significant increase in observed fluorescence compared to the Δ*msrC* mutant but not significantly different from the WVC in 1 mM H_2O_2 (Figure 21B). This suggests that MsrC in *K. hansenii* plays a role in ROS tolerance and defence. This is analogous to what has been reported for *S. cerevisiae* where different combinations of deletions of *Msr* genes lead to decreased survivability under oxidative stress tested with 1.2 mM and 1.5 mM exogenous H_2O_2 (Le *et al.,* 2009). This infers that MsrC contributes to a broader network of genes and proteins involved in managing ROS levels in *K. hansenii.*

In terms of ROS tolerance, the pUCD2::*msrC* complementation construct was not able to fully restore tolerance to ROS as shown by the survivability assay in Figure 22. Although not being statistically significant, it was observed that the WT was able to survive in all concentrations of H_2O_2 and even show an increase in survivability at 5 mM compared to 3 mM. The Δ*msrC* mutant and MVC were unable to survive in 3 mM and 5 mM H_2O_2 with increased lethality at 1 mM H_2O_2. The fact that WT survivability increased at 5 mM H_2O_2 relative to 3 mM H_2O_2 may point to a hermetic response, where low doses of a stressor enhance the organism's ability to cope with higher levels of stress. However, without MsrC, the cells appear to lack the necessary adaptive response.

In all, the data suggests that while the pUCD2::*msrC* complementation construct enhances ROS tolerance relative to the Δ*msrC* mutant, it does not completely replicate the WT phenotype. The differential ROS management between the strains could be due to the dosage or expression levels of the MsrC protein from the complementation construct, which may not fully match those of the native gene within the WT strain. It may also indicate the involvement of additional, as yet unidentified, genetic elements or regulatory pathways that interact with MsrC to mediate a comprehensive response to oxidative stress. These findings give us a glimpse of the functional role of MsrC in oxidative stress resistance in *K. hansenii* and suggest potential avenues for further research. For example, examining the expression levels and activity of the MsrC protein in the complemented strain could help elucidate the reasons behind the incomplete restoration of the WT phenotype. In addition, exploration of the regulatory networks that govern the expression and activity of MsrC may uncover as yet unidentified components of the oxidative stress response in this organism.

Since the biofilm mode of growth is integral for the survival of *Komagataeibacter* spp. as evidenced by the constitutive production of protective cellulose, and since quorum sensing plays a fundamental role in microbial community dynamics, it was of interest to explore how the manipulation of MsrC, a potentially key enzyme involved in methionine salvage, might intersect with, and potentially influence, AHL-mediated communication in *K. hansenii.*

Through the experiments described in this thesis, it was found that antibiotic carryover of spectinomycin and chloramphenicol impacted the biosensing capability of *R. radiobacter* (Figure 23 A & B). Most studies reported in the literature have used this

biosensor as a screening tool of unmodified environmental bacteria or have used it to sense AHLs in purified extracts. Given that the literature does not extensively report what antibiotics *R. radiobacter* is sensitive to, which, as a biosensor, is important to know especially when working with mutations that require antibiotic selections, this thesis highlights the importance of understanding these sensitivities when using *R. radiobacter* as a biosensor, particularly in mutation studies requiring antibiotic selection. To reduce the need to retest AHL production in future experiments, MICs of the selective antibiotics used to maintain any mutations or plasmids (if any) should be performed on *R. radiobacter* to determine if compensations need to be made such as cultivation without antibiotics.

When cultivated in the absence of antibiotics, unexpected differences in the amounts of AHLs between the five strains (WT, Δ*msrC*, WVC, MVC, and complement) were observed (Figure 23C). The WT was not shown in Figure 23C since it was already grown without antibiotics and it showed AHL production not significantly different from the *P. aeruginosa* supernatant allowing the latter to be used as a surrogate for WT in the comparative analysis.

The Δ*msrC* mutant and MVC showed increased AHL secretion compared to the WVC and complement (Figure 23). The increase in AHL production of the Δ*msrC* mutant could explain the increase in cellulose production as observed in Figure 13. It has been observed in acetic acid bacteria that AHLs are needed for cellulose production, with obstruction of AHL communication leading to disruption of pellicle synthesis (Liu *et al.*, 2019). Even though cellulose is typically constitutively synthesized by *K. hansenii* and other *Komagataeibacter* species, it is also subject to regulation and can be influenced by

various environmental factors (Arbing 2020, Augimeri and Strap 2015, Quereshi et. al. 2013). If cellulose synthesis, and by extension pellicle production, is modulated in a dose dependent manner due to AHL communication, the large increase in AHL secretion in the Δ*msrC* mutant may be why it was able to produce more pellicle. The MVC produced relatively the same amount of AHLs as the Δ*msrC* mutant, however it produced less pellicle which implies that there is something else besides AHLs that are lowering cellulose yield, potentially including the presence of the pUCD2 plasmid. The complement showed decreased AHL emission to levels similar to the WVC, and significantly different than the Δ*msrC* mutant or the MVC. This shows that MsrC plays a role in regulating AHL-mediated cellular communication. With the current data, it is unclear whether MsrC is responsible for regulating production of AHLs or for expediting AHL excretion. This could be tested by comparing the amount of AHLs produced by the WT and Δ*msrC* when cells are lysed, to allow for AHLs held within the cell cytoplasm and periplasmic space to be released in the supernatant and be detected by *R. radiobacter*.

A possible explanation for the incomplete restoration of WT phenotypes with the complement is that there may be a regulatory discrepancy between the native *msrC* in the WT compared to the complement. As mentioned above, there may be other regulatory elements involved with *msrC* that are either missing or unable to act on the pUCD2::*msrC* complementation construct. This can be verified by quantitative reverse transcriptase PCR (qRT-PCR) to compare the transcription of *msrC* in the WT to that of the complement strain.

Given that there are observable impacts of the pUCD2 plasmid, the selective antibiotics, and/or the medium used for antibiotic delivery, a future avenue of

investigation for *msrC* would be creating a clean-deletion mutant. This would involve introducing a truncated DNA sequence of the *msrC* gene with homologous ends to *K. hansenii,* similar to the method described in section 1.13 (Figure 7). Ideally, *K. hansenii* will recognize the homologous ends of the truncated gene and incorporate it into its genome via homologous recombination, simultaneously removing the native *msrC* gene. This would result in a Δ*msrC* mutant that does not need antibiotic selection and does not have non-native DNA inserted into *K. hansenii* that might mask the effects of the gene deletion. The clean deletion method would also allow for a much simpler complementation to verify the mutation by re-introducing the native *msrC* gene in the same manner as the truncated gene and observe whether WT phenotypes can be restored compared to the new Δ*msrC* mutant.

Chapter 5. Conclusions

The goal of this thesis was to functionally characterize the GAF-domain-containing MsrC protein in *Komagataeibacter hansenii.* Growth analysis of the five *K. hansenii* strains (WT, Δ*msrC*, WVC, MVC, and complement) shows that MsrC helps regulate the growth of *K. hansenii*. Morphological analysis shows an observable decrease in cell size variability in the Δ*msrC*, indicating that MsrC regulates the cell length of *K. hansenii*. When exposed to the phytohormones, MsrC has been found to participate in the response system to ABA. Evaluating intracellular ROS levels using DCF shows that MsrC affects homeostatic ROS levels in *K. hansenii*. Currently, it is unknown if MsrC plays a role in ethylene detection despite possessing similar characteristics to plant based ethylene receptors. The pUCD2 shuttle vector has been found to have multiple impacts

on *K. hansenii* such as pH 7 tolerance, variable effects on cellulose production, and can impact transformants differently.

K. hansenii has been shown to secrete AHLs in its environment as detected by *R. radiobacter* and that the pUCD2::*msrC* complementation construct reduced AHL signalling. This shows that MsrC is involved in AHL based quorum sensing. The biosensor *R. radiobacter* has been shown to have sensitivity to the antibiotics chloramphenicol and spectinomycin to the extent of impeding its ability to detect AHLs. When detecting the induction of LacZ by *R. radiobacter* it has been found that there is no advantage between measuring absorbance with 615 nm or 660 nm.

Therefore, we propose that MsrC has a survival role in *K. hansenii* for dealing with pH stress and oxidative stress. It also is a growth coordinator, phytohormone response agent and quorum sensing regulator. Despite all the findings uncovered in this thesis, there is the possibility to discover more with MsrC and warrants further investigation.

REFERENCES

Al-Janabi, S. S., Shawky, H., El-Waseif, A. A., Farrag, A. A., Abdelghany, T. M., & El-Ghwas, D. E.(2022). Novel approach of amplification and cloning of bacterial cellulose synthesis (BCS) operon from *Gluconoacetobacter hansenii*. *Gene Reports, 27*, 101577.https://doi.org/10.1016/j.genrep.2022.101577

Arbing, J. (2020). Characterization of a carbon source-dependent, phytohormone-responsive, free methionine-(R)-sulfoxide reductase from *Komagataeibacter hansenii*.

Augimeri, R. V. (2016). Ethylene response and phytohormone-mediated regulation of gene expression in *Komagataeibacter xylinus* ATCC 53582.

Augimeri R. V. & Strap J. L. (2015). The phytohormone ethylene enhances cellulose production, regulates CRP/FNRKx transcription and causes differential gene expression within the bacterial cellulose synthesis operon of *Komagataeibacter (Gluconacetobacter) xylinus* ATCC53582. *Frontiers in Microbiol*ogy. 6:1459. doi: 10.3389/fmicb.2015.01459

Augimeri, R. V., Varley, A. J., & Strap, J. L. (2015). Establishing a role for bacterial cellulose in environmental interactions: Lessons learned from diverse biofilm-producing proteobacteria. *Frontiers in Microbiology*, *6*. https://doi.org/10.3389/fmicb.2015.01282

Balagurumoorthy, P., Adelstein, S. J., & Kassis, A. I. (2008). Method to eliminate linear DNA from mixture containing nicked circular, supercoiled, and linear plasmid DNA. *Analytical Biochemistry*, *381*(1), 172–174. https://doi.org/10.1016/j.ab.2008.06.037

Binder, B. M. (2007). The ethylene receptors: Complex perception for a simple gas. *Plant Science*, *175*(1-2), 8–17. https://doi.org/10.1016/j.plantsci.2007.12.001

Boukraa, M., Sabbah, M., Soulère, L. E. l., Efrit, M. L., Queneau, Y., & Doutheau, A. (2011). AHL-dependent quorum sensing inhibition: Synthesis and biological evaluation of α-(N-alkyl-carboxamide)-γ-butyrolactones and α-(N-alkyl-sulfonamide)-γ-butyrolactones. *Bioorganic & Medicinal Chemistry Letters*, *21*(22), 6876–6879. https://doi.org/10.1016/j.bmcl.2011.09.010

Calderón-Toledo, S., Horue, M., Alvarez, VA., Castro, G. R., & Zavaleta, A. I. (2021). Isolation and partial characterization of *Komagataeibacter* SP.. su12 and optimization of bacterial cellulose production using *Mangifera indica* extracts. *Journal of Chemical Technology & Biotechnology*, *97*(6), 1482–1493. https://doi.org/10.1002/jctb.6839

Cepec, E., & Trček, J. (2022). Antimicrobial resistance of Acetobacter and *Komagataeibacter* species originating from vinegars. *International Journal of Environmental Research and Public Health*, *19*(1), 463. https://doi.org/10.3390/ijerph19010463

Cheon, B. & Gladyshev, B. (2011). The biological significance of methionine sulfoxide stereochemistry. *Free Radic Biol Med*, vol. 50, no. 2, pp. 221–227., https://doi.org/10.1016/j.freeradbiomed.2010.11.008.

Christmann, A., Weiler, E. W., Steudle, E., & Grill, E. (2007). Hydraulic signal in root-to-shoot signalling of water shortage. *The Plant Journal: For Cell and Molecular Biology*, *52*(1), 167–174. https://doi.org/10.1111/j.1365-313X.2007.03234.x

Chu, D., Huang, Z., & He, F. (2018). Comparison between sulfuric acid-phenol and sulfuric acid-anthrone methods used for determination of polysaccharides in shoots of *Aralia elata* (Miq.) Seem. *Agricultural Biotechnology (Pawtucket, R.I.)*, *7*(3), 170–173

Cruz, C. G., Rosa, A. P. C., & Costa, J. A. V. (2023). Identification of the phytohormones indole-3-acetic acid and trans-zeatin in microalgae. *Journal of Chemical Technology and Biotechnology (1986)*, *98*(4), 1048–1056. https://doi.org/10.1002/jctb.7312

Deng, Y., Nagachar, N., Fang, L., Luan, X., Catchmark, J. M., Tien, M., & Kao, T. (2015). Isolation and characterization of two cellulose morphology mutants of *Gluconacetobacter hansenii* ATCC23769 producing cellulose with lower crystallinity. PloS One, 10(3), e0119504–. https://doi.org/10.1371/journal.pone.0119504

Elías, J. M., Guerrero-Molina, M. F., Martínez-Zamora, M. G., Díaz-Ricci, J. C., & Pedraza, R. O. (2018). Role of ethylene and related gene expression in the interaction between strawberry plants and the plant growth-promoting bacterium *Azospirillum brasilense*. *Plant Biology*, *20*(3), 490–496. https://doi.org/10.1111/plb.12697

Feehily, C., & Karatzas, K. A. G. (2013). Role of glutamate metabolism in bacterial responses towards acid and other stresses. *Journal of Applied Microbiology*, *114*(1), 11–24. https://doi.org/10.1111/j.1365-2672.2012.05434.x

Fischer, A. J., Rockwell, N. C., Jang, A. Y., Ernst, L. A., Waggoner, A. S., Duan, Y., Lei, H., & Lagarias, J. C. (2005). Multiple roles of a conserved GAF domain tyrosine residue in cyanobacterial and plant phytochromes. *Biochemistry (Easton)*, *44*(46), 15203–15215. https://doi.org/10.1021/bi051633z

Flemming, H.-C., & Wingender, J. (2010). The biofilm matrix. *Nature Reviews. Microbiology*, *8*(9), 623–633. https://doi.org/10.1038/nrmicro2415

Guzman, P., & J. R Ecker. Exploiting the triple response of *Arabidopsis* to identify ethylene-related mutants. *Plant Cell*, vol. 2, no. 6, 1990, pp. 513–523., https://doi.org/10.1105/tpc.2.6.513.

Hestrin, S., & Schramm, M. (1954). Synthesis of cellulose by *Acetobacter xylinum* . 2. Preparation of freeze-dried cells capable of polymerizing glucose to cellulose. *Biochemical Journal*, *58*(2), 345–352. https://doi.org/10.1042/bj0580345

Galperin, M. Y. (2004), Bacterial signal transduction network in a genomic perspective. *Environmental Microbiology*, 6: 552-567. https://doi.org/10.1111/j.1462-2920.2004.00633.x

Gamper, N., & Shapiro, M. S. (2007). Regulation of ion transport proteins by membrane phosphoinositides. *Nature Reviews. Neuroscience*, *8*(12), 921–934. https://doi.org/10.1038/nrn2257

Gurgel, L. V. A., Marabezi, K., Zanbom, MD., & Curvelo, AA da S. (2012). Dilute acid hydrolysis of sugar cane bagasse at high temperatures: A kinetic study of cellulose saccharification and glucose decomposition. Part I: Sulfuric acid as the catalyst. *Industrial & Engineering Chemistry Research*, *51*(3), 1173–1185. https://doi.org/10.1021/ie2025739

Hirayama, T., & Alonso, J. M. (2000). Ethylene captures a metal! Metal ions are involved in ethylene perception and signal transduction. *Plant and Cell Physiology*, *41*(5), 548–555. https://doi.org/10.1093/pcp/41.5.548

Ho, Y.-S. J., Burden, L. M., & Hurley, J. H. (2001). Structure of the GAF domain, a ubiquitous signaling motif and a new class of cyclic GMP receptor. *The EMBO Journal*, *20*(6), 1483–1483. https://doi.org/10.1093/emboj/20.6.1483

Imlay, J. A. (2013). The molecular mechanisms and physiological consequences of oxidative stress: lessons from a model bacterium. *Nature Reviews Microbiology*, *11*(7), 443–454. https://doi.org/10.1038/nrmicro3032

Imlay, J. A., & Fridovich, I. (1991). Assay of metabolic superoxide production in *Escherichia coli*. *The Journal of Biological Chemistry*, *266*(11), 6957–6965. https://doi.org/10.1016/S0021-9258(20)89596-9

Jakubowski, Witold, and Grzegorz Bartosz. 2,7-Dichlorofluorescin oxidation and reactive oxygen species: What does it measure? *Cell Biol Int*, vol. 24, no. 10, 2000, pp. 757–760., https://doi.org/10.1006/cbir.2000.0556.

Jayabalan., Malbaša, Lončar, Vitas, & Sathishkumar, M. (2014). A review on kombucha tea-microbiology, composition, fermentation, beneficial effects, toxicity, and tea fungus. *Comprehensive Reviews in Food Science and Food Safety*, *13*(4), 538–550. https://doi.org/10.1111/1541-4337.12073

Kappus & Sies, (1981). Toxic drug effects associated with oxygen metabolism: redox cycling and lipid peroxidation. *Experientia*, *37*(12), 1233–1241. https://doi.org/10.1007/BF01948335

Kaur, T., & Manhas, R. K. (2022). Evaluation of ACC deaminase and indole acetic acid production by *Streptomyces hydrogenans* DH16 and its effect on plant growth

promotion. *Biocatalysis and Agricultural Biotechnology*, *42*, 102321–. https://doi.org/10.1016/j.bcab.2022.102321

Kim, J. S., Kim, T. L., Kim, K. C., Choe, C., Chung, H. W., Cho, E. W., & Kim, I. G. (2006). S-Adenosylmethionine decarboxylase partially regulates cell growth of HL-60 cells by controlling the intracellular ROS level: Early senescence and sensitization to γ-radiation. *Archives of Biochemistry and Biophysics*, *456* (1), 58–70. https://doi.org/10.1016/j.abb.2006.09.020

Kornmann, H., Duboc, P., Niederberger, P., Marison, I., & Stockar, U. von. (2003). Influence of residual ethanol concentration on the growth of *Gluconacetobacter xylinus* I 2281. *Applied Microbiology and Biotechnology*, 62 (2/3), 168–173. https://doi.org/10.1007/s00253-003-1299-2

Kumar, A., Toledo, J. C., Patel, R. P., Lancaster, J. R., & Steyn, A. J. C. (2007). *Mycobacterium tuberculosis* DosS is a redox sensor and DosT is a hypoxia sensor. *Proceedings of the National Academy of Sciences - PNAS*, *104* (28), 11568–11573. https://doi.org/10.1073/pnas.0705054104

Lacey, Randy F, and Brad M Binder. Ethylene regulates the physiology of the *Cyanobacterium synechocystis* Sp. PCC 6803 via an ethylene receptor. *Plant Physiol*, vol. 171, no. 4, 2016, pp. 2798–2809., https://doi.org/10.1104/pp.16.00602.

Lacey, Randy F, and Brad M Binder. How plants sense ethylene gas — The ethylene receptors. *Journal of Inorganic Biochemistry*, vol. 133, 2014, pp. 58–62., https://doi.org/10.1016/j.jinorgbio.2014.01.006.

Lacey, R. F., Allen, C. J., Bakshi, A., & Binder, B. M. (2018). Ethylene causes transcriptomic changes in Synechocystis during phototaxis. *Plant Direct*, *2*(3), e00048-n/a. https://doi.org/10.1002/pld3.48

Laursen, B. S., Sørensen, H. P., Mortensen, K. K., & Sperling-Petersen, H. U. (2005). Initiation of protein synthesis in bacteria. *Microbiology and Molecular Biology Reviews*, *69*(1), 101–123. https://doi.org/10.1128/MMBR.69.1.101-123.2005

Le, D. T., Lee, B. C., Marino, S. M., Zhang, Y., Fomenko, D. E., Kaya, A., Hacioglu, E., Kwak, G.-H., Koc, A., Kim, H.-Y., & Gladyshev, V. N. (2009). Functional analysis of free methionine-R-sulfoxide reductase from *Saccharomyces cerevisiae*. *The Journal of Biological Chemistry*, *284*(7), 4354–4364. https://doi.org/10.1074/jbc.M805891200

Lin, Z., Johnson, L. C., Weissbach, H., Brot, N., Lively, M. O., & Lowther, W. T. (2007). Free methionine-(R)-sulfoxide reductase from *Escherichia coli* reveals a new GAF domain function. *Proceedings of the National Academy of Sciences - PNAS*, *104*(23), 9597–9602. https://doi.org/10.1073/pnas.0703774104

Liu, L.-P., Huang, L.-H., Ding, X.-T., Yan, L., Jia, S.-R., Dai, Y.-J., Xie, Y.-Y., & Zhong, C. (2019). Identification of quorum-sensing molecules of N -Acyl-Homoserine Lactone in *Gluconacetobacter* strains by liquid chromatography-

tandem mass spectrometry. *Molecules (Basel, Switzerland)*, *24*(15), 2694–. https://doi.org/10.3390/molecules24152694

Lohani, S., Trivedi, P. K., & Nath, P. (2004). Changes in activities of cell wall hydrolases during ethylene-induced ripening in banana: effect of 1-MCP, ABA and IAA. *Postharvest Biology and Technology*, *31*(2), 119–126. https://doi.org/10.1016/j.postharvbio.2003.08.001

Lowther, W. T., Brot, N., Weissbach, H., & Matthews, B. W. (2000). Structure and mechanism of peptide methionine sulfoxide reductase, an "anti-oxidation" enzyme. *Biochemistry (Easton)*, *39*(44), 13307–13312. https://doi.org/10.1021/bi0020269

Matsushita, K.,Inoue, T., Adachi, O., & Toyama, H. (2005). *Acetobacter aceti* possesses a proton motive force-dependent efflux system for acetic acid. *Journal of Bacteriology*, *187*(13), 4346–4352. https://doi.org/10.1128/JB.187.13.4346-4352.2005

Milić, D., Dick, M., Mulnaes, D., Pfleger, C., Kinnen, A., Gohlke, H., & Groth, G. (2018). Recognition motif and mechanism of ripening inhibitory peptides in plant hormone receptor ETR1. *Scientific Reports*, *8*(1), 3890–12. https://doi.org/10.1038/s41598-018-21952-3

Miyazaki, & S.F Yang. The methionine salvage pathway in relation to ethylene and polyamine biosynthesis. *Physiologia Plantarum*, vol. 69, no. 2, 1987, pp. 366–370., https://doi.org/10.1111/j.1399-3054.1987.tb04302.x.

Paldrychová, M., Vaňková, E., Scholtz, V., Julák, J., Sembolová, E., Mat'átková, O., & Masák, J. (2019). Effect of non-thermal plasma on AHL-dependent QS systems and biofilm formation in Pseudomonas aeruginosa: Difference between non-hospital and clinical isolates. *AIP Advances*, *9*(5), 055117–055117–7. https://doi.org/10.1063/1.5090451

Pardoux, R., Dolla, A., & Aubert, C. (2021). Metal-containing PAS/GAF domains in bacterial sensors. *Coordination Chemistry Reviews*, *442*, 214000-. https://doi.org/10.1016/j.ccr.2021.214000

Paul, R., Weiser, S., Amiot, N. C., Chan, C., Schirmer, T., Giese, B., & Jenal, U. (2004). Cell cycle-dependent dynamic localization of a bacterial response regulator with a novel di-guanylate cyclase output domain. *Genes & Development*, *18*(6), 715–727. https://doi.org/10.1101/gad.289504

Prakash Singh, M., & Greenstein, M. (2006). A simple, rapid, sensitive method detecting homoserine lactone (HSL)-related compounds in microbial extracts. *Journal of Microbiological Methods*, *65*(1), 32–37. https://doi.org/10.1016/j.mimet.2005.06.003

Puelles, L., Diaz, C., Stühmer, T., Ferran, J. L., Martínez-de la Torre, M., & Rubenstein, J. L. R. (2021). LacZ-reporter mapping of Dlx5/6 expression and genoarchitectural analysis of the postnatal mouse prethalamus. *Journal of Comparative Neurology (1911)*, *529*(2), 367–420. https://doi.org/10.1002/cne.24952

Qureshi, O., Sohail, H., Latos, A., & Strap, J. L. (2013). The effect of phytohormones on the growth, cellulose production and pellicle properties of *Gluconacetobacter xylinus* ATCC 53582. *Acetic Acid Bacteria*, *2*(s1), e7. https://doi.org/10.4081/aab.2013.s1.e7

Rabbani, M., Maruyama, K., Abe, H., Khan, M. ., Katsura, K., Ito, Y., Yoshiwara, K., Seki, M., Shinozaki, K., & Yamaguchi-Shinozaki, K. (2003). Monitoring expression profiles of rice genes under cold, drought, and high-salinity stresses and abscisic acid application using cDNA microarray and RNA gel-blot analyses. *Plant Physiology (Bethesda)*, *133*(4), 1755–1767. https://doi.org/10.1104/pp.103.025742

Ramachandran, S., Loganathan, S., Cheeran, V., Charles, S., Munuswamy-Ramanujan, G., Ramasamy, M., Raj, V., & Mala, K. (2018). Forskolin attenuates doxorubicin-induced accumulation of asymmetric dimethylarginine and S-adenosylhomocysteine via methyltransferase activity in leukemic monocytes. *Leukemia Research Reports*, *9*, 28–35. https://doi.org/10.1016/j.lrr.2018.02.001

Rodrigues, A. M. S., Lami, R., Escoubeyrou, K., Intertaglia, L., Mazurek, C., Doberva, M., Pérez-Ferrer, P., & Stien, D. (2022). Straightforward N-acyl homoserine lactone discovery and annotation by LC–MS/MS-based molecular networking. *Journal of Proteome Research*, *21*(3), 635–642. https://doi.org/10.1021/acs.jproteome.1c00849

Ryjenkov, D. A.,Tarutina, M., Moskvin, O. V., & Gomelsky, M. (2005). Cyclic diguanylate is a ubiquitous signaling molecule in bacteria: Insights into biochemistry of the GGDEF protein domain. *Journal of Bacteriology*, *187*(5), 1792–1798. https://doi.org/10.1128/JB.187.5.1792-1798.2005

Saeki, A. Yamaguchi-ken. G. O., Matsushita, K., Takeno, S., Taniguchi, M., Toyama, H., Theeragool, G., Lotong, N., & Adachi, O. (1999). Enzymes responsible for acetate oxidation by acetic acid bacteria. *Bioscience, Biotechnology, and Biochemistry*, 63(12), 2102–2109. https://doi.org/10.1271/bbb.63.2102

Schneider, C.A., Rasband, W.S., Eliceiri, K.W. NIH Image to ImageJ: 25 years of image analysis. *Nature Methods* 9, 671-675, 2012.

Soto, E., Ortega-Ramírez, A., & Vega, R. (2018). Protons as messengers of intercellular communication in the nervous system. *Frontiers in Cellular Neuroscience*, *12*, 342–342. https://doi.org/10.3389/fncel.2018.00342

Su, Y., & Lagarias, J. C. (2007). Light-Independent phytochrome signaling mediated by dominant GAF domain tyrosine mutants of *Arabidopsis* phytochromes in transgenic plants. *The Plant Cell*, *19*(7), 2124–2139. https://doi.org/10.1105/tpc.107.051516

Valera, M. J., Torija, M. J., Mas, A., & Mateo, E. (2015). Acetic acid bacteria from biofilm of strawberry vinegar visualized by microscopy and detected by complementing culture-dependent and culture-independent techniques. *Food Microbiology*, *46*, 452–462. https://doi.org/10.1016/j.fm.2014.09.006

Weinhouse, H., Sapir, S., Amikam, D., Shilo, Y., Volman, G., Ohana, P., & Benziman, M. (1997). c-di-GMP-binding protein, a new factor regulating cellulose synthesis in *Acetobacter xylinum*. *FEBS Letters*, *416*(2), 207–211. https://doi.org/10.1016/S0014-5793(97)01202-7

Wong, H. C., Fear, A. L., Calhoon, R. D., Eichinger, G. H., Mayer, R., Amikam, D., Benziman, M., Gelfand, D. H., Measde, J. H., Emerick, A. W., Bruner, R., Ben-Bassat, A., & Tal, R. (1990). Genetic organization of the cellulose synthase operon in *Acetobacter xylinum. Proceedings of the National Academy of Sciences*, *87*(20), 8130–8134. https://doi.org/10.1073/pnas.87.20.8130

Xiaoman Q., Yao X., & Housheng H. Classification of acetic acid bacteria and their acid resistant mechanism. AMB Expr (2021) 11:29

Zhao, Y.-Q., Hu, K.-D., Yao, G.-F., Wang, S.-Y., Peng, X.-J., & Zhang, H. (2023). A D-cysteine desulfhydrase, SlDCD2, participates in tomato fruit ripening by modulating ROS homoeostasis and ethylene biosynthesis. *Horticulture Research*, *10*(3). https://doi.org/10.1093/hr/uhad014

Ziesche, L., Rinkel, J., Dickschat, J. S., & Schulz, S. (2018). Acyl-group specificity of AHL synthases involved in quorum-sensing in *Roseobacter* group bacteria. *Beilstein Journal of Organic Chemistry*, *14*(1), 1309–1316. https://doi.org/10.3762/bjoc.14.112

Appendix A.

A.1 Glucose Equivalence Determination by Anthrone Standard Curve

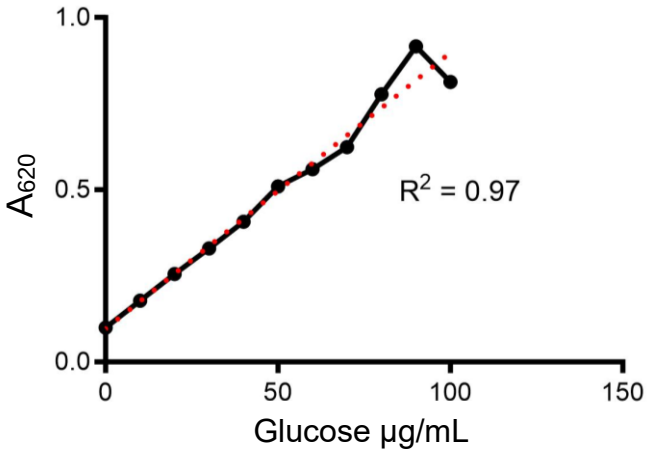

Figure A1. Standard curve for determination of glucose concentration in µg/mL). Experiments were done in triplicate n=3. R^2 value for line of best fit = 0.97.